Reviews in Mineralogy & Geochemistry
Vol. 86 pp. 367–400, 2021

Triple Oxygen Isotopes in Silica–Water and Carbonate–Water Systems

Jordan A.G. Wostbrock* and Zachary D. Sharp

Department of Earth and Planetary Sciences
University of New Mexico
Albuquerque, NM 87131
USA

jogibbons7@unm.edu

zsharp@unm.edu

INTRODUCTION

The field of stable isotope geochemistry began with the recognition that the oxygen isotope composition of ancient carbonates could be used as a paleothermometer (Urey 1947; Urey et al. 1951). As stated by Urey (1947), "*Accurate determinations of the O^{18} content of carbonate rocks could be used to determine the temperature at which they were formed"*. This concept was based on the temperature dependence for the oxygen isotope fractionation between calcite and water. Urey realized that if a mass spectrometer with sufficient precision could be built, a method of reproducibly extracting oxygen from solid carbonate could be developed, and the isotope fractionations between calcite and water could be quantified, then the oxygen isotope composition of ancient carbonates could be used to determine the temperature of their formation.

This idea led to the carbonate–water temperature scale (McCrea 1950; Epstein et al. 1951, 1953; Urey et al. 1951). The oxygen isotope compositions of marine carbonates are sensitive to temperature (increase with decreasing formation temperature), so that ancient seawater temperatures could be determined by measuring the oxygen isotope composition of the carbonate. Urey et al. (1951) recognized a number of potential problems with the carbonate thermometer, including: 1) the possibility that organisms form out of oxygen isotope equilibrium, a term he called the '*vital effect*'; 2) the possibility that shells might not preserve their oxygen isotope composition over geological time and undergo some sort of post-mortem diagenesis; and 3) the uncertainty in the estimate of the oxygen isotope composition of the formation water. To this last point, the oxygen isotope composition of the ancient seawater is estimated and not measured directly. What is the possibility that the ocean has changed its oxygen isotope composition through time? Urey et al. (1951) concluded that any significant changes would have occurred before the Cambrian, although he states that '*it is a conclusion based on little more than prejudice*'. In spite of these caveats, the carbonate paleothermometer has been immensely successful and applied in many thousands of studies. It also led to the development of other mineral–water thermometers such as silica–water thermometry. However, the concerns raised by Urey remain, despite numerous efforts to ascertain diagenesis and quantify any changes in the ocean oxygen isotope composition through time. Recently, the rare $^{17}O/^{16}O$ ratio has begun to be measured and included in geologic studies. The addition of this new variable has allowed researchers to discern equilibrium vs. disequilibrium processes governing precipitation of a mineral and determine whether alteration occurred in a sample after its initial precipitation.

1529-6466/21/0086-0011$05.00 (print)
1943-2666/21/0086-0011$05.00 (online)
http://dx.doi.org/10.2138/rmg.2021.86.11

While triple oxygen isotope measurements (measuring both the $^{17}O/^{16}O$ and $^{18}O/^{16}O$ ratios) have been performed on a variety of materials, this chapter reviews the current literature on the triple oxygen isotope fractionation between silica–water and carbonate–water. An overview of both equilibrium and disequilibrium fractionation is given through theory, empirical calibrations, and laboratory experiments. We then apply these different fractionation regimes to geologic samples. We also give a brief overview of how the silica–water and calcite–water triple oxygen isotope fractionation curves can be used to reconstruct past seawater oxygen isotope values. We conclude the chapter by calculating and discussing potential uses of a quartz–calcite fractionation curve.

MINERAL–WATER OXYGEN ISOTOPE THERMOMETERS

$^{18}O/^{16}O$ fractionation

Oxygen isotope paleothermometers are based on the temperature dependent fractionation between authigenic minerals and their formation water. For marine sediments, we generally assume that the formation water is seawater and that the oxygen isotope composition of the seawater has not varied through time. Obviously, this is a critical assumption that has been questioned and evaluated extensively and is discussed later in this chapter. Oxygen isotope paleothermometers have been developed for carbonates, silicates, phosphates and sulfates. In this communication, we address only the silica–water and carbonate–water paleotemperature equations. We begin with an overview of the generic $^{18}O/^{16}O$ thermometer.

One of the first calibrations of the calcite–water oxygen isotope thermometer took the form (Epstein et al. 1951, 1953)

$$t\,(^{\circ}\mathrm{C}) = 16.5 - 4.3\,\delta + 0.14\,\delta^2 \tag{1}$$

In this equation δ is the isotopic composition of the CO_2 evolved from the carbonate relative to the δ value of CO_2 evolved from a reference carbonate (Peedee belemnite or PDB). The $\delta^{18}O$ value is defined, in per mil (‰) notation, as

$$\delta^{18}\mathrm{O} = \left(\frac{R_{\mathrm{sa}}}{R_{\mathrm{std}}} - 1\right) \times 1000 \tag{2}$$

where R is the $^{18}O/^{16}O$ ratio of the sample (sa) and standard (std). A similar equation can be written for the $\delta^{17}O$ value, in which case R is the $^{17}O/^{16}O$ value.

Equation (1) is simply a quadratic best fit to empirical data and is not based on any theoretical considerations. Bigeleisen and Goeppert Mayer (1947) showed that the log of the equilibrium fractionation between diatomic molecules should be proportional to T^{-1} and T^{-2} (in Kelvin) at low and high temperatures, respectively. The system becomes more complicated with more complex phases, especially when water is considered (Criss 1991). Empirical data are often fit to $1/T$, $1/T^2$ or a combination of these two. In mineral–water fractionation equations, a constant is often included as a consequence of the high vibrational frequencies of water (Bottinga and Javoy 1973). An appropriate fit to the temperature dependence of fractionation between phase i and water is given by:

$$1000 \ln \alpha_{i-\mathrm{H_2O}} = \frac{a \times 10^6}{T^2} + c \tag{3}$$

Here $\alpha_{i-\mathrm{H_2O}} = \dfrac{R_i}{R_{\mathrm{H_2O}}}$ and in delta notation $\alpha_{i-\mathrm{H_2O}} = \dfrac{1000 + \delta_i}{1000 + \delta_{\mathrm{H_2O}}}$. An alternative form for mineral–water fractionation is to add a $1/T$ term to the equation (e.g., Zheng 1991):

$$1000\ln\alpha_{i-H_2O} = \frac{a\times10^6}{T^2} + \frac{b\times10^3}{T} + c \quad (4)$$

The constant in Equations (3) and (4) lead to equations that are not valid at high temperatures because $1000\ln\alpha$ values approach zero, and not c, at infinite temperatures. An alternative expression is to fit the data to a polynomial of $1/T$, such as

$$1000\ln\alpha_{i-H_2O} = \frac{a\times10^6}{T^2} + \frac{b\times10^3}{T} \quad (5)$$

The justification of using the form of Equation (3) is apparent when we consider actual data. Figure 1 shows experimental and empirical fractionation data for quartz–water and carbonate–water as a function of $1/T^2$. The data are approximated by a linear fit and a y intercept (the c term in Eqn. 3) of 3.4‰ (quartz) and 2.95‰ (calcite) (Fig. 1A). Obviously, this relationship fails at very high temperatures, where the $1000\ln\alpha$ must approach zero. A better fit is expected if we use a polynomial of $1/T$ and $1/T^2$ as predicted from theory (Clayton and Kieffer 1991). A polynomial fit for quartz–water and carbonate–water is shown in Figure 1B. The constant is zero in these fits so that $1000\ln\alpha$ goes to infinity at infinite temperatures. Both curves have the same general sigmoidal form, indicating that the constant in Equation (3), which is likely valid at lower temperatures (e.g., Bottinga and Javoy 1973) must decrease with increasing temperature.

The quartz–water system has been experimentally and empirically studied over a uniquely wide temperature range. Quartz–water exchange experiments have been made between 250 °C and 800 °C (see Sharp et al. 2016 for a compilation). Low temperature empirical fractionation of diatoms and abiogenic silica have been measured over the temperature range of 0 to almost 100 °C (Kita et al. 1985; Leclerc and Labeyrie 1987; Shemesh et al. 1995; Brandriss et al. 1998; Schmidt et al. 2001; Dodd and Sharp 2010). All low- and high-temperature quartz–water fractionation data can be fit to Equation (5), where a = 4.28 ± 0.07 and b = −3.5 ± 0.2 (R^2 = 0.9978) (Sharp et al. 2016). Eliminating the c constant allows for the fractionation equation to be extrapolated to infinite temperature. In contrast, carbonate–water experimental and empirical data are better fit to the form of Equation (3) up to ~1000 K (O′Neil et al. 1969; Wostbrock et al. 2020b). Equation (5) does not adequately fit both the high temperature experimental results and low temperature synthesis and empirical data. In this paper we use the general form of Equation (4). Based only on fitting published fractionation data, we set the c term to zero for quartz–water, and the b term to zero for carbonate–water.

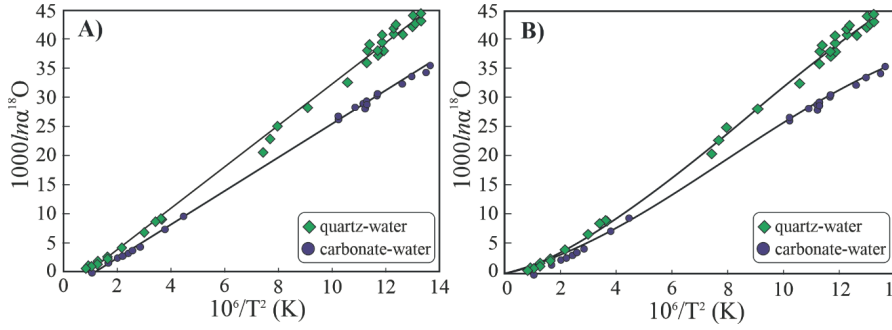

Figure 1. Quartz–water (**green diamond**) and calcite–water (**blue circle**) oxygen isotope fractionation. **A)** Best fit using Equation (3) ($a \times 10^6/T^2 + c$) with a negative y-intercept. **B)** Best fit using Equation (5) ($a \times 10^6/T^2 + b \times 10^3/T$) and a y-intercept of zero. The quartz–water data are better approximated by Equation (5) (Fig. 1B), whereas the carbonate–water data is better fit by Equation (3). Higher order polynomial fits are not warranted, as the errors in the coefficients become very large.

Triple oxygen isotope fractionation

The equilibrium fractionation of $^{17}O/^{16}O$ relative to $^{18}O/^{16}O$ between two phases A and B is given by the equation

$$\alpha^{17}O_{A-B} = \left(\alpha^{18}O_{A-B}\right)^{\theta} \quad (6)$$

In a linearized format, where $\delta' = 1000 \ln(\delta/1000 + 1)$ (Hulston and Thode 1965; Miller 2002), $\delta'_A - \delta'_B = 1000 \ln \alpha_{A-B}$ and Equation (6) can be recast as

$$\delta'^{17}O_A - \delta'^{17}O_B = \theta(\delta'^{18}O_A - \delta'^{18}O_B) \quad (7)$$

The θ value varies with temperature ranging from 0.5305 at $T = \infty$ to 0.526, 0.524, and 0.518 – 0.52 at $T = 298$ K for calcite–water (Wostbrock et al. 2020b), quartz–water (Cao and Liu 2011; Sharp et al. 2016; Hayles et al. 2018), and quartz–calcite (Hayles et al. 2018 and this chapter), respectively. To a first approximation, the temperature dependence of θ for phases A and B is given by (Sharp et al. 2016)

$$\theta_{A-B} = 0.5305 - \frac{\varepsilon}{T} \quad (8)$$

where ε is a constant, although higher order polynomials are indicated from theory (Cao and Liu 2011; Hayles et al. 2018; Guo and Zhou 2019). Combining Equations (4), (7) and (8) gives the equilibrium $\delta^{17}O$ fractionation equation between phases A and B:

$$1000 \ln \alpha_{A-B}^{^{17}O/^{16}O} = \delta'^{17}O_A - \delta'^{17}O_B = \left(\frac{a \times 10^6}{T^2} + \frac{b \times 10^3}{T} + c\right)\left(0.5305 - \frac{\varepsilon}{T}\right) \quad (9)$$

For all terrestrial samples not affected by mass independent fractionation processes (e.g., Thiemens 2006), $\delta'^{17}O$ varies with $\delta'^{18}O$ by the empirical equation known as the *Terrestrial Fractionation Line* or TFL

$$\delta'^{17}O = \lambda \delta'^{18}O + \gamma \quad (10)$$

In Equation (10), λ is an empirical best fit to natural data and not tied to any thermodynamic relationship and γ is the *y* intercept that is generally assumed to be zero. Similar to other chapters in this volume, throughout this work we use a λ value of 0.528.

Departures from the linear relationship given in Equation (10) are subtle and expressed using the $\Delta'^{17}O$ value, given by the equation

$$\Delta'^{17}O = \delta'^{17}O - \lambda \delta'^{18}O \quad (11)$$

The equations governing the mineral–water isotope fractionation for the three oxygen isotopes are the following:

$$\delta'^{18}O_{mineral} = \delta'^{18}O_{water} + \frac{a \times 10^6}{T^2} + \frac{b \times 10^3}{T} + c \quad (12)$$

$$\delta'^{17}O_{mineral} = \delta'^{17}O_{water} + \left(\frac{a \times 10^6}{T^2} + \frac{b \times 10^3}{T} + c\right)\left(0.5305 - \frac{\varepsilon}{T}\right) \quad (13)$$

and

$$\Delta'^{17}O_{mineral} = \delta'^{17}O_{water} - \lambda \cdot \delta'^{18}O_{water} + \left(\frac{a \times 10^6}{T^2} + \frac{b \times 10^3}{T} + c\right)\left(0.5305 - \frac{\varepsilon}{T} - \lambda\right) \quad (14)$$

For minerals in equilibrium with seawater similar to Standard Mean Ocean Water (SMOW, $\delta^{17}O = \delta^{18}O = 0$), Equation (14) reduces to

$$\Delta'^{17}O_{mineral} = \left(\frac{a\times10^6}{T^2} + \frac{b\times10^3}{T} + c\right)\left(0.5305 - \frac{\varepsilon}{T} - \lambda\right) \quad (15)$$

Combining Equations (12) and (13) allows us to calculate the relationship between the $\Delta'^{17}O$ and $\delta'^{18}O$ values of a mineral (subscript r) in equilibrium with water (subscript w). The solution is the following:

$$\Delta'^{17}O_r = \delta'^{17}O_w + \left(\delta'^{18}O_r - \delta'^{18}O_w\right)\times \left(0.5305 + \frac{\left(c - \delta'^{18}O_r + \delta'^{18}O_w\right)\varepsilon}{500\left(b + \sqrt{b^2 - 4a\left(c - \delta'^{18}O_r + \delta'^{18}O_w\right)}\right)} - \lambda\right) - \delta'^{18}O_w\cdot\lambda \quad (16)$$

Equilibrium triple oxygen isotope fractionation—the $\Delta'^{17}O$–$\delta'^{18}O$ plot

The benefit of the triple oxygen isotope system is apparent when we plot the $\Delta'^{17}O$ value of a mineral against the $\delta'^{18}O$ value using Equation (16) (Fig. 2). The triple oxygen isotope plot ($\Delta'^{17}O$ *vs.* $\delta'^{18}O$) allows us to clearly distinguish equilibrium or disequilibrium precipitation for a given sample. Figure 2 is constructed for quartz in equilibrium with ocean water, but an equally relevant figure could be generated for calcite or any other low temperature phase for which triple oxygen isotope fractionation data are available. The solid black curve represents the locus of $\delta'^{18}O$ and $\Delta'^{17}O$ values of silica in equilibrium with seawater equal to SMOW (yellow star). All silica samples in oxygen isotope equilibrium with SMOW must plot on the solid black curve. Note, that seawater with a $\delta^{18}O$ value of 0‰ and $\Delta'^{17}O$ value of –0.005‰ can also be used to represent seawater based on Luz and Barkan (2010). In this chapter, we clearly state whether we are using seawater with a $\Delta'^{17}O$ value of 0 or –0.005‰. Equilibrium temperatures (in °C) decrease along the curve with increasing $\delta'^{18}O$ values and decreasing $\Delta'^{17}O$ values.

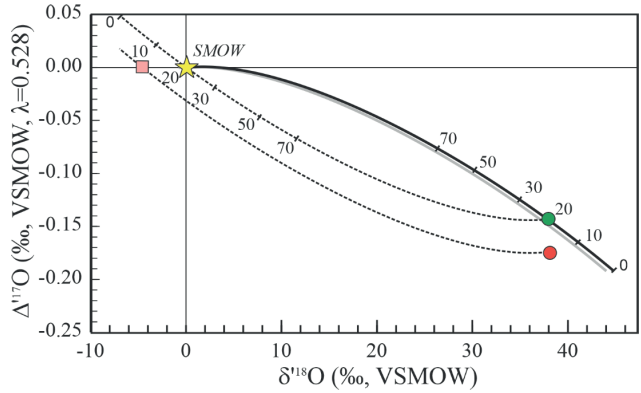

Figure 2. $\Delta'^{17}O$–$\delta'^{18}O$ plot for silica–water. The **solid black curve** shows the combined $\Delta'^{17}O$–$\delta'^{18}O$ values of silica in equilibrium with SMOW (Standard Mean Ocean Water, $\delta^{18}O = \Delta'^{17}O = 0$). The position along the line is determined by the temperature of equilibration. The **grey line** is for a seawater with a $\delta'^{18}O$ value of –1‰ (ice free conditions). The **dashed curves** are the same as the equilibrium fractionation curve (**black solid curve**) only inverted. The curve's origin is placed at the silica triple oxygen isotope value and the dashed lines represent the water in equilibrium with the silica. The **red and green circles** represent two hypothetical samples. The **dashed line emanating from the green circle** passes through the seawater composition with a 20 °C temperature. The **dashed line from the red circle** does not intersect seawater. Therefore, the sample represented by the red circle cannot be in equilibrium with seawater at any temperature. It could be in equilibrium with a different water composition, such as the **pink square**.

The triple oxygen isotope values of two hypothetical samples are shown in Figure 2 by the red and green circles. Both have $\delta'^{18}O$ values of 37.9‰. With $\delta'^{18}O$ values alone, the two samples are indistinguishable and correspond to a formation temperature of 20 °C. The addition of the $\Delta'^{17}O$ value clearly provides more information. The green circle lies on the equilibrium curve, suggesting that the sample is indeed in equilibrium with seawater at 20 °C. The red circle does not plot on the seawater equilibrium curve. *Therefore, this sample cannot be in equilibrium with seawater* ($\delta^{18}O$ and $\Delta'^{17}O = 0$) *at any temperature.* Adding the ^{17}O isotope unambiguously demonstrates disequilibrium precipitation with modern seawater and/or equilibrium precipitation with a different water oxygen isotope composition. Lowering the $\delta^{18}O$ value of the ocean by ~1‰ during interglacial periods is shown by the grey equilibrium curve (Fig. 2). The $\Delta'^{17}O$ value of an ice-free ocean should be close to 0, so the curve moves to −1‰ and does not explain the position of the red circle. As described later in this chapter, the region where the red circle plots in Figure 2 is diagnostic of diagenesis.

The quartz-seawater equilibrium curve (solid grey and black curves; Fig. 2) can be inverted such that the origin of the curve is placed on the measured $\delta'^{18}O$–$\Delta'^{17}O$ value of the sample (dashed lines; Fig. 2). In this case, the dashed line defines the water composition in equilibrium with that sample. For the green circle, the intersection of the dashed line with SMOW occurs at 20 °C, the apparent equilibrium temperature. The dashed line emanating from the red circle does not pass through SMOW, again indicating that there is no temperature at which this sample can be in equilibrium with seawater. The red circle could be in equilibrium with a water having a $\delta^{18}O$ value of –5‰ and $\delta'^{17}O$ value of 0‰ (pink square; Fig. 2) or any water with a triple oxygen isotope value the plots on the dashed line emanating from the red circle.

KINETIC EFFECTS RESULTING IN OXYGEN ISOTOPE DISEQUILIBRIUM

Rapid precipitation of a mineral at low temperature may result in kinetic effects that lead to disequilibrium oxygen isotope fractionations. The effect was recognized in the first synthesis study of calcite for the purpose of determining the $\alpha^{18}O_{CaCO_3–H_2O}$ fractionation (McCrea 1950). He found that the $\delta^{18}O$ value of rapidly precipitated calcite approached that of the carbonate ion in solution. Disequilibrium has been seen in many natural samples as well. Cave calcite (speleothems) and travertines can precipitate out of oxygen isotope equilibrium due to rapid CO_2 degassing (Gonfiantini et al. 1968; Mickler et al. 2006; Carlson et al. 2020). Biogenic calcite can precipitate out of oxygen isotope equilibrium due to the rapid precipitation of calcite resulting in incomplete equilibration between the carbonate ion CO_3^{2-} and water (McConnaughey 1989), or by changing the relative concentrations of the dissolved carbonate species by changing *p*H (Spero et al. 1997; Zeebe 1999). On the basis of clumped carbonate isotope measurements (Δ_{47}), it has been suggested that most natural calcites are out of oxygen isotope equilibrium (Daëron et al. 2019).

The problem appears to be minimal for the silica–water system. Silica–water fractionations are mostly insensitive to biogenic *vs*. abiogenic conditions (Shemesh et al. 1992; Wostbrock et al. 2018), although there is clear evidence that diatoms precipitate out of equilibrium with water (Schmidt et al. 1997, 2001; Dodd et al. 2012). However, diatoms appear to re-equilibrate with water within a year post-mortem (Dodd et al. 2012; Tyler et al. 2017). The general insensitivity of silica precipitation to kinetic isotope effects is probably related to the simple chemistry of precipitation. Silica forms from H_4SiO_4 with an intermediate $SiOOH^+$ ion (Crundwell 2017). Solubilities of quartz are extremely low at *p*H below 9 with H_4SiO_4 being the principle dissolved species (Krauskopf 1956). Precipitation is generally slow, so that there is minimal disequilibrium between the dissolved species and crystallizing silica.

Disequilibrium effects with dissolved inorganic carbon

Carbonates, on the other hand, have been shown on numerous occasions to precipitate out of thermodynamic equilibrium (Gonfiantini et al. 1968; Shackleton et al. 1973; McConnaughey 1989; Kim and O′Neil 1997; Spero et al. 1997; Zeebe 1999, 2014; Mickler et al. 2004, 2006; Beck et al. 2005; Dietzel et al. 2009; Tremaine et al. 2011; Watkins et al. 2013; Devriendt et al. 2017; Bajnai et al. 2018; Daëron et al. 2019; Carlson et al. 2020). The primary complication that exists for carbonates is that the oxygen isotope fractionation is not simply controlled by the water oxygen isotope composition, but rather by the fractionation between calcite and all dissolved inorganic carbon (DIC) species: $CO_{2(aq)}$, H_2CO_3, HCO_3^-, and CO_3^{2-}. The relevant proportions of these DIC species are strongly controlled by *p*H, and there is a large oxygen isotope fractionation between them. The $1000 \ln \alpha^{18}O$ values (at 25 °C) range from 31.1‰ for HCO_3^-–H_2O to 24.2‰ for CO_3^{2-}–H_2O (Beck et al. 2005). Combining these results with the $\alpha_{calcite–water}$ demonstrates that HCO_3^- has a higher $\delta^{18}O$ value than coexisting calcite, whereas CO_3^{2-} has a much lower $\delta^{18}O$ value than calcite. Dissolved inorganic carbon is mainly present as HCO_3^- at intermediate *p*H, but CO_3^{2-} at high *p*H.

When all species are in oxygen isotope equilibrium, *p*H has no effect on fractionation between calcite and water. Calcite precipitation is governed by the reaction (Garrels and Christ 1965)

$$Ca^{2+} + CO_3^{2-} = CaCO_3 \tag{17}$$

and, as long as the CO_3^{2-} ion is in equilibrium with water, and calcite precipitates in equilibrium with all DIC species, then the calcite is also in equilibrium with water. The equilibrium $\delta^{18}O$ value of all dissolved carbonate species is determined by the $\delta^{18}O$ value of water, which is overwhelmingly the predominant oxygen reservoir.

Several phenomena lead to disequilibrium oxygen isotope values during calcite precipitation. First, a transient disequilibrium between the dissolved carbonate species and water will occur if the *p*H of the system is rapidly changed. This happens for example, when CO_2 is added to or lost from the system. When subterranean CO_2-saturated waters reach the surface, they rapidly degas CO_2, *p*H increases and calcite (travertine) precipitates. Second, kinetic effects at the surface of a growing calcite crystal may lead to non-equilibrium if the rates of incorporation and detachment of the HCO_3^- and CO_3^{2-} ions into the carbonate lattice are different (Watkins et al. 2013). Because the relative proportions of DIC species are strongly controlled by *p*H, the $\delta^{18}O$ values of some shell-secreting organisms are affected by the *p*H of the solution (Spero et al. 1997; Zeebe 1999; Adkins et al. 2003).

For the reaction

$$HCO_3^- \leftrightarrow H^+ + CO_3^{2-} \tag{18}$$

isotopic equilibrium is reached almost instantaneously because the protonation of CO_3^{2-} and deprotonation of HCO_3^- are extremely rapid. Equilibration between the bicarbonate ion and water and dissolved CO_2 (or H_2CO_3) occurs far more slowly. Equilibrium between H_2O and DIC will occur via CO_2 hydration and hydroxylation by the reactions

$$CO_2 + H_2O \leftrightarrow H_2CO_3 \leftrightarrow H^+ + HCO_3^- \tag{19}$$

and

$$CO_2 + OH^- \leftrightarrow HCO_3^- \tag{20}$$

Equation (19) controls equilibration rates at moderate *p*H, Equation (20) becomes important at high *p*H with higher OH^- concentrations. Oxygen isotope equilibration between H_2O and DIC requires hours to days, depending on temperature and *p*H (Mills and Urey 1940; McConnaughey 1989; Beck et al. 2005; Uchikawa and Zeebe 2012; Watkins et al. 2013)[1].

[1] Mills and Urey (1940) found very similar rates for DIC–water equilibration as later work.

The $\delta^{18}O$ value of the sum of the hydrated DIC species is given by

$$\delta^{18}O_{\Sigma(DIC)} = \frac{\left(\delta^{18}O_{H_2CO_3}\right)\left[H_2CO_3\right] + \left(\delta^{18}O_{HCO_3^-}\right)\left[HCO_3^-\right] + \left(\delta^{18}O_{CO_3^{2-}}\right)\left[CO_3^{2-}\right]}{\left[H_2CO_3\right] + \left[HCO_3^-\right] + \left[CO_3^{2-}\right]} \quad (21)$$

where the square brackets are the concentration of the dissolved species (Zeebe 1999). Note that dissolved CO_2 is not considered in our computation of the $\delta^{18}O_{\Sigma(DIC)}$ value. If all dissolved species are in equilibrium with water, then the $\delta^{18}O_{\Sigma(DIC)}$ value will change with *p*H (Fig. 3). At low *p*H (below about 6.5), the $\delta^{18}O_{\Sigma(DIC)}$ value will be equal to that of H_2CO_3 ($\delta^{18}O = 39.5‰$), which makes up the vast majority of the total DIC. At very high *p*H (above about 9), the $\delta^{18}O_{\Sigma(DIC)}$ value will be equal to the CO_3^{2-} ion ($\delta^{18}O = 18.4‰$), which is the predominant DIC species. If the relative incorporation of the DIC species into the carbonate lattice is kinetically controlled, then the oxygen isotope composition of the precipitating calcite will be affected by *p*H. If *all* DIC were to be incorporated into a fast-growing calcite, then the $\delta^{18}O$ value of the calcite would simply equal the $\delta^{18}O_{\Sigma(DIC)}$. In Figure 3, the $\delta^{18}O$ value of the calcite would track along the $\delta^{18}O_{\Sigma(DIC)}$ curve (thick black line). Spero et al. (1997) and Bijma et al. (1999) found a clear linear relationship between *p*H and the $\delta^{18}O$ values of foraminifera, independent of symbiont activity and temperature. There is a well-established kinetic-based *p*H–$\delta^{18}O$ relationship for carbonates that is controlled by non-equilibrium fractionation during hydration and hydroxylation of CO_2 or by rate-dependent incorporation of different DIC components.

Oxygen isotope disequilibrium can occur due to rapid CO_2 degassing or ingassing, such as production or consumption of CO_2 within the cell membranes by respiration (McConnaughey 1989). Some researchers suggest that slowly precipitated calcites in caves closer represent thermodynamic calcite–water equilibrium, represented by the higher $1000 \ln \alpha_{calcite-water}$ values than that of most biogenic calcite and laboratory precipitation experiments (Coplen 2007; Tremaine et al. 2011; Daëron et al. 2019).

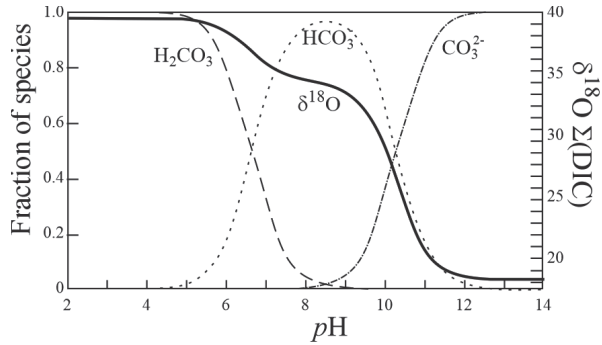

Figure 3. Effect of *p*H on the relative abundance of DIC species and on the $\delta^{18}O$ value of total dissolved inorganic carbon. At low *p*H the $\delta^{18}O_{\Sigma(DIC)}$ is nearly identical to that of the H_2CO_3 species ($\delta^{18}O = 39.5‰$), whereas at very high *p*H, it is equal to that of the CO_3^{2-} ion ($\delta^{18}O = 18.4‰$). The above diagram is calculated assuming oxygen isotope equilibrium and the total DIC concentration $\Sigma[DIC] = [H_2CO_3] + [HCO_3^-] + [CO_3^{2-}]$. For this example, $\delta^{18}O_{water} = 0‰$, $T = 25$ °C, isotope fractionation data from Zeebe (1999).

Application to the triple oxygen isotope system

Guo and Zhou (2019) estimated both equilibrium and kinetic triple oxygen isotope fractionations in the H_2O–DIC–CO_2 system using $\ln \alpha^{18}O_{eq}$ values between dissolved carbonate species from earlier theoretical estimates (Hill et al. 2014). The triple oxygen isotope exponent, κ, is similar for all dissolved carbonate species and calcite, but different for CO_2 ($\kappa = \ln^{17}\beta / \ln^{18}\beta$,

and is equivalent to the θ value between the phase and monoatomic oxygen; Cao and Liu 2011). They considered three processes that would disturb the equilibrium conditions of a system and modelled how the triple oxygen isotope system evolved as it returned to equilibrium. The three processes are: 1) a sudden change in DIC oxygen isotope composition due to dissolution of a water-soluble carbonate, 2) a rapid loss of CO_2 by degassing, and 3) an increase in CO_2 concentration (AKA ingassing or absorption) as might occur inside a cell during CO_2 respiration.

When the system is perturbed, the $\delta^{18}O$ and $\delta^{17}O$ values of all DIC species initially change and, over time, return to oxygen isotope equilibrium with the water. However, the rates of exchange are different for ^{17}O and ^{18}O, so that there are subtle variations in the θ and $\Delta'^{17}O$ values of the dissolved carbonate species during the perturbation (Fig. 4). The pathways shown in Figure 4 illustrate the transient changes in the $\delta^{18}O$ and $\Delta'^{17}O$ values of HCO_3^-. We can consider the HCO_3^- ion to control the $\delta^{18}O$ value of the carbonate triple oxygen isotope composition during one of these perturbation episodes at moderate *p*H (6.5–9) and temperature (20–30 °C). Rapid loss of CO_2 increases the θ, $\Delta'^{17}O$, and $\delta^{18}O$ values (Fig. 4), which then return to equilibrium over a period of several hours. Absorption of CO_2 has the opposite effect, lowering the θ, $\Delta'^{17}O$ and $\delta^{18}O$ values (Fig. 4) which again return to equilibrium in several hours. Changing the DIC concentration and oxygen isotope composition (by addition of sodium bicarbonate in the example) results in a curved trajectory in $\Delta'^{17}O$–$\delta^{18}O$ space (Fig. 4) where the θ and $\Delta'^{17}O$ values initially increase, and then decrease while the $\delta^{18}O$ values continuously decreases and whole system approaches equilibrium over a period of several hours to days (depending on *p*H and temperature).

As an example, rapid surface degassing of a subterranean fluid with high $p(CO_2)$ will raise the *p*H of the fluid and cause rapid deposition of carbonates (travertines). The red curve in Figure 4 shows that under such a degassing process, we might expect the $\delta^{18}O$ and $\Delta'^{17}O$ values to increase. Preliminary results of the triple oxygen isotope composition of travertines from actively precipitating 10–20 °C springs in Tierra Amarilla, NM have higher $\Delta'^{17}O$ and $\delta'^{18}O$ values, 0.05‰ and 2–5‰, respectively, than expected from equilibrium precipitation from its formation fluid (unpublished results from a senior thesis at the University of New Mexico).

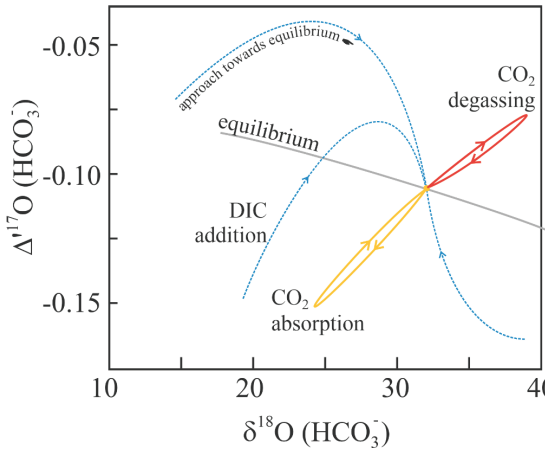

Figure 4. Changes in the $\delta^{18}O$ and $\Delta'^{17}O$ values of dissolved HCO_3^- during degassing of CO_2 (**red curve**), absorption of CO_2 (**yellow curve**) and introduction of a disequilibrium source of DIC (such as dissolution of Na_2CO_3–**blue dashed curves**). The starting point of the equilibration path following introduction of DIC (blue curves) is controlled by the $\delta^{18}O$ and $\Delta'^{17}O$ of the starting DIC, as illustrated by three different starting points. Figure is reformatted after modelling data in Guo and Zhou (2019). Temperature, *p*H and isotopic composition of the water also have an effect.

Fosu et al (2020) measured the triple oxygen isotope composition of a large variety of carbonates and found a surprisingly wide range of $\Delta'^{17}O$ values. For example, they measured two cold seep carbonates with $\Delta'^{17}O$ values that differed by 0.13‰ between each other. This is more than double the $\Delta'^{17}O$ range of carbonate samples thought to be in equilibrium with seawater (see Fig. 13 later in this chapter). Cold seep carbonates have been shown to be out of clumped isotope equilibrium (Loyd et al. 2016). One cold seep sample has a $\Delta'^{17}O$ value that is about 0.05‰ higher than the $\Delta'^{17}O$ equilibrium value expected with seawater while the other sample has a $\Delta'^{17}O$ value that is 0.10‰ lower than expected for equilibrium formation with seawater ($\delta^{17}O = \delta^{18}O = \Delta'^{17}O = 0$). Perhaps the triple oxygen isotope compositions are also showing disequilibrium values. Research addressing how disequilibrium processes affect the triple oxygen isotope values of the precipitating mineral is clearly an area of future research.

SILICA–WATER FRACTIONATION

Calibration of the triple oxygen isotope silica–water thermometer

The $^{18}O/^{16}O$ fractionation between silica and water and its temperature dependence is extremely well studied. There are at least 7 experimental fractionation studies of quartz–water at high temperatures (see Sharp et al. 2016 for a compilation) and a number of empirical studies of naturally-formed abiogenic and biogenic amorphous silica at low to moderate temperatures (Kita et al. 1985; Leclerc and Labeyrie 1987; Shemesh et al. 1995; Brandriss et al. 1998; Schmidt et al. 2001; Dodd and Sharp 2010). Low temperature diatom silica initially form out of equilibrium with their host water (Brandriss et al. 1998; Dodd and Sharp 2010), but then undergo an early maturation phase, such that the silica reaches oxygen isotope equilibrium within the first year or two post-mortem (Schmidt et al. 2001; Dodd et al. 2012; Tyler et al. 2017).

Wostbrock et al. (2018) compared the triple oxygen isotope values of abiogenic and biogenic silica as well as amorphous and microcrystalline silica and found no measurable differences in the $\delta^{18}O$ fractionation. Therefore, we include both the high temperature equilibration experiments and the low temperature empirical fractionation data from biogenic and abiogenic silica to derive an SiO_2–H_2O oxygen isotope fractionation equation valid at temperatures above 273 K, given by

$$1000 \ln \alpha^{18}O_{SiO_2-H_2O} = \frac{4.28 \times 10^6}{T^2} - \frac{3500}{T} \quad (22)$$

The low temperature anchor on Equation (22) is primarily controlled by Antarctic diatom data. Shemesh et al. (1992) recommended only using Antarctic diatoms for the empirical silica–water fractionation to avoid complications of upwelling effects seen in other regions. Equation (22) fits the published low temperature diatom data well (Fig. 5), suggesting that the equation is valid down to 0 °C.

The temperature dependent $^{17}O/^{16}O$ fractionation for quartz–water has been determined empirically by measuring the triple oxygen isotope compositions of quartz and abiogenic and biogenic amorphous silica (coexisting water was also measured when possible) over a temperature range of 0 to over 100 °C (Sharp et al. 2016; Wostbrock et al. 2018). The θ–*T* relationship can be calculated using Equation (8) with the best fit given by

$$\theta_{qz-wt} = 0.5305 - \frac{1.85}{T} \quad (23)$$

The θ–*T* results are shown in Figure 6 along with two theoretical calibrations (Cao and Liu 2011; Hayles et al. 2018). There is generally good agreement between the empirical and theoretical estimates, with the latter having slightly higher θ values at low temperatures.

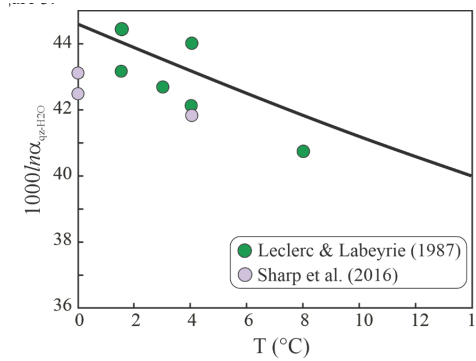

Figure 5. Comparison of the quartz–water fractionation equation (**solid curve**) with low temperature diatom data (Leclerc and Labeyrie 1987; Sharp et al. 2016). All analyses fit the equation to within 4 °C.

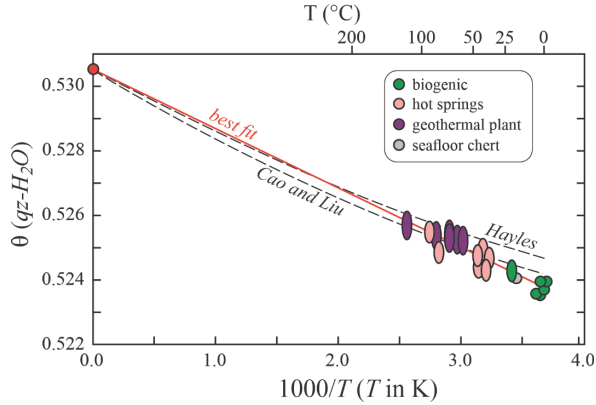

Figure 6. Measured θ values for natural samples and best fit for a θ *vs.* 1/*T* relationship. Data from Sharp et al. (2016) and Wostbrock et al. (2018). Also shown are the theoretical curves of Cao and Liu (2011) and Hayles et al. (2018).

The $\Delta\Delta'^{17}O$ fractionations ($\Delta'^{17}O_{silica} - \Delta'^{17}O_{water}$) as a function of temperature are governed by Equation (14). For silica–water, we have

$$\Delta'^{17}O_{silica} = \delta'^{17}O_{water} - \lambda \cdot \delta'^{18}O_{water} + \left(\frac{4.28\times10^{6}}{T^{2}} + \frac{3.5\times10^{3}}{T}\right)\left(0.5305 - \frac{1.85}{T} - \lambda\right) \quad (24)$$

where λ is assigned a value of 0.528 in this chapter. Equation (24) allows us to construct the $\Delta'^{17}O$–$\delta'^{18}O$ equilibrium curves for silica–water (Fig. 2).

Silica in the terrestrial environment

Figure 7 shows the quartz–water triple oxygen isotope plot with the equilibrium curves inverted (dashed lines) so that the origin is placed at the silica oxygen isotope composition for three silica samples. This allows us to estimate the oxygen isotope compositions of the formation waters in a terrestrial (non-marine) setting in equilibrium with a given silica sample. The green diamond is a modern sinter (amorphous silica) from Yellowstone National Park, Wyoming. Both the neoform silica and coexisting water (green circle) were sampled. A water temperature of 47 °C was measured at the time of collection. The silica and water appear to be in triple oxygen isotope equilibrium. They both lie on the same equilibrium curve with a

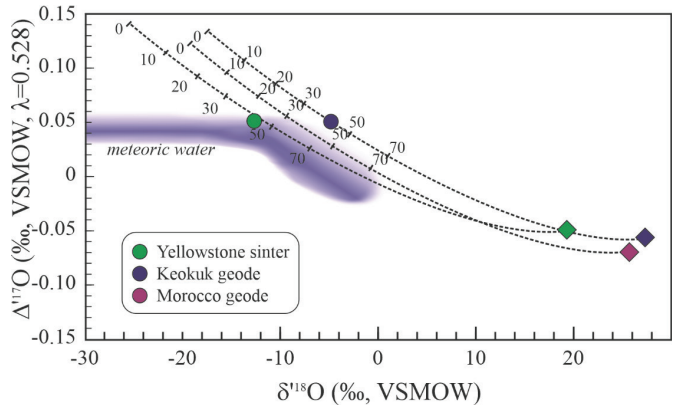

Figure 7. Triple isotope compositions of low-*T* terrestrial silica samples. Data from Sharp et al. (2016). The Yellowstone sinter and Keokuk geode have oxygen isotope data for the coexisting waters and correspond to formation temperatures of 40–50 °C. The Moroccan geode has a similar oxygen isotope composition to the other two samples suggesting similar conditions of formation. Meteoric water field from Sharp et al. (2018).

corresponding temperature of 42 °C. The measured water is ~10‰ higher than local meteoric water, suggesting the sampled water has undergone some degree of evaporation and/or hydrothermal exchange with the host rock. The blue diamond is microcrystalline quartz from a Keokuk geode that retained fossil water in its core (blue circle). We do not know if the core water represents the formation water. However, the triple oxygen isotope values for the quartz and the water do in fact suggest equilibrium at a temperature of ~45 °C, suggesting the core water could be representative of the initial formation water. The purple diamond is microcrystalline quartz found in a stalactitic geode from Morocco (Sharp et al. 2016). We do not have coexisting water for this sample, but recognizing the $\Delta'^{17}O$ value of the sample is slightly lower than the other two samples, we estimate a formation temperature of ~40 °C. Data from all the samples suggest that crystalline quartz can form at temperatures as low as 40 to 50 °C.

CARBONATE–WATER FRACTIONATION

Analytical method

The standard method for determining the $\delta^{18}O$ value of carbonates was derived in 1950 (McCrea 1950). Carbonates are reacted with 100% phosphoric acid at a constant temperature, producing CO_2 gas from the breakdown of the carbonate. Only 2/3 of the oxygen in the carbonate is liberated as CO_2 gas. However, if the decarbonation is performed at a constant temperature, then the fractionation ($\delta^{18}O_{CO_2\,(ACID)}$–$\delta^{18}O_{carbonate}$ or $\alpha_{CO_2\,(ACID)–carbonate}$) should be constant, although there are subtle second order effects that should be considered (Sharp 2017). In order to calculate the actual $\delta^{18}O$ value of the carbonate on the VSMOW-SLAP scale, it is necessary to know the $\alpha_{CO_2\,(ACID)–carbonate}$ fractionation factor (Sharp and Wostbrock 2021, this volume). This value is determined by liberating 100% of the oxygen from the carbonate either through complete fluorination of the carbonate (Sharma and Clayton 1965) or decarbonation of the carbonate as CO_2 followed by fluorination of the remaining CaO (Kim and O'Neil 1997; Kim et al. 2007). In these carbonate studies, CO_2 and/or a combination of CO_2 and O_2 gas were produced. The O_2 was converted to CO_2 by reaction with a heated graphite rod and all CO_2 was recombined for the measurement of the $\delta^{18}O$ value of the total carbonate. The difference between the $\delta^{18}O$ values of the CO_2 produced by reaction with phosphoric acid and of the total carbonate gives us the $\alpha^{18}O_{CO_2\,(ACID)–carbonate}$ value.

These procedures cannot be used to determine the $\delta^{17}O$ value of carbonates. There is an isobaric interference at mass 45 ($^{12}C^{16}O^{17}O$) by ^{13}C ($^{13}C^{16}O^{16}O$). The $\delta^{17}O$ value must be measured on O_2 gas unless an ultra-high precision mass spectrometer is being used that can measure the O^+ fragment of CO_2 (Adnew et al. 2019). The problem with extracting O_2 gas from carbonates by fluorination is that intermediate compounds, such as CO and COF_2, are produced and they are very resistant to fluorination. Wostbrock et al. (2020a) modified the Sharma and Clayton (1965) procedure of carbonate fluorination to quantitatively extract O_2. The method involves conventional fluorination in Ni reaction tubes heated to 750 °C for four days. Wostbrock et al. (2020a) measured the triple oxygen isotope values of international standards as well as the CO_2 liberated by phosphoric acid digestion. These data provide us with the $\alpha^{17}O_{CO_2\ (ACID)–carbonate}$ value of 1.00535 when using the $\alpha^{18}O_{CO_2\ (ACID)–carbonate}$ value of 1.01025 (Wostbrock et al. 2020a) . With these data, other laboratories that indirectly measure the $\delta^{17}O$ value of CO_2 generated by phosphoric acid digestion can calculate the $\delta^{17}O$ value of the total carbonate. Alternative methods that start with the CO_2 gas released by phosphoric acid digestion include the following: converting CO_2 to H_2O followed by fluorination (Passey et al. 2014), equilibrating CO_2 gas with O_2 using a hot Pt catalyst (Mahata et al. 2013; Barkan et al. 2015; Fosu et al. 2020), and analyzing the O^+ fragment of CO_2 generated in the ion source using a high resolution mass spectrometer (Adnew et al. 2019). Laser spectroscopy that measures the $\delta^{17}O$ value of CO_2 is a promising new technology that has yet to be adapted to wide-scale use (Sakai et al. 2017). We refer readers to Passey and Levin (2021, this volume) and Sharp and Wostbrock (2021, this volume) for more information about procedures used to measure the triple oxygen isotope values of carbonates.

Triple oxygen isotope fractionation in the calcite (aragonite)–water system

Debate is ongoing regarding which type of carbonate (synthetic, biogenic, or abiogenic) best represents equilibrium oxygen isotope fractionation (Coplen 2007; Bajnai et al. 2018; Brand et al. 2019) or if naturally forming carbonates even reach equilibrium with the waters in which they form (Daëron et al. 2019). Wostbrock et al. (2020b) examined each category of carbonates (biogenic marine carbonate, biogenic and abiogenic marine aragonite, abiogenic Devils Hole calcite, synthesized calcite with and without carbonic anhydrase) to determine differences in triple oxygen isotope fractionation using the carbonate fluorination method. The synthesis experiments consisted of slowly precipitating calcite at a constant temperature following the method of Kim and O′Neil (1997) either with or without carbonic anhydrase (CA) as a catalyst (Silverman 1973; Uchikawa and Zeebe 2012; Watkins et al. 2013). The natural samples included marine biogenic calcite and marine abiogenic and biogenic aragonite that had known water $\delta^{18}O$ values and growth temperatures. They found no statistically significant difference in the $1000 \ln \alpha^{18}O_{cc\text{-}wt}$ between synthetic, biogenic, and abiogenic calcite or aragonite but the $1000 \ln \alpha^{18}O_{cc\text{-}wt}$ values were at the higher end of that in reported literature ($1000 \ln \alpha^{18}O_{carb\text{-}wt} = 29.0$ at 25 °C). Wostbrock et al. (2020b) used all the samples from each category, combined with high temperature experimental data from O′Neil et al. (1969) to derive the $1000 \ln \alpha^{18}O_{carb\text{-}wt}$ portion of the triple oxygen isotope fractionation (Eqn. 14) given by

$$1000 \ln \alpha^{^{18}O/^{16}O}_{carb-water} = \frac{2.84 \times 10^6}{T^2} - 2.96 \tag{25}$$

A difference was seen in the $1000 \ln \alpha^{17}O$ values between calcite–water and aragonite–water (Wostbrock et al. 2020b). Calcite–water has higher θ values and smaller $\Delta\Delta'^{17}O_{carb–wt}$ ($\Delta'^{17}O_{carbonate} - \Delta'^{17}O_{water}$) values than aragonite–water (Fig. 8). However, these conclusions are based on aragonite samples from a very narrow range of temperatures (25–26 °C) and should be considered preliminary until a wider temperature range is measured. The calcite–water triple oxygen isotope fractionation equation from Wostbrock et al. (2020b) is:

$$\Delta'^{17}O_{carb} - \Delta'^{17}O_{wt} = \left(\frac{2.84\times10^{6}}{T^{2}} - 2.96\right)\left(\frac{-1.39}{T} + 0.5305 - \lambda\right) \quad (26)$$

It is unclear whether any of the carbonates presented in Wostbrock et al. (2020b) represents true thermodynamic equilibrium. Isotopic equilibrium will not be reached in a natural setting if there is disequilibrium between the dissolved carbonate species (see earlier section "*Effects of dissolved inorganic carbon*"). If one of the dissolved species is out of equilibrium with the others and with the water, then the precipitated carbonate may reflect that disequilibrium (Guo and Zhou 2019). Regardless of whether Equation (26) represents 'true' thermodynamic equilibrium or not, it does show a correlation between $\Delta\Delta'^{17}O_{carb-wt}$ and temperature that should be applicable any naturally formed carbonates.

The triple oxygen isotope fractionation equations for calcite have also been calculated from theory (Cao and Liu 2011; Hayles et al. 2018; Guo and Zhou 2019). There is a systematic increase in the $\Delta\Delta'^{17}O_{carb-wt}$ value as a function of decreasing temperature, similar to what is seen for quartz and what is predicted from theory (Fig. 8; Hayles et al. 2018; Guo and Zhou 2019). As noted earlier, there was no statistical difference in the $\Delta\Delta'^{17}O_{carb-wt}$ values between the different calcite groups presented in Wostbrock et al. (2020b). There was a statistical difference between the calcite samples (blue circles and squares, Fig. 8) and the aragonite samples (brown circles, Fig. 8) where the best fit of the aragonite samples (brown line, Fig. 8) is lower at all temperatures, compared to the best fit of the calcite samples (blue line, Fig. 8). The calcite results agree well with theoretical estimates (black line, Fig. 8; Hayles et al. 2018; Guo and Zhou 2019). However, theoretical calculations predict there to be little to no difference between the $\Delta'^{17}O$ values of aragonite and calcite (Guo and Zhou 2019; Schauble and Young 2021, this volume).

Two other studies (Bergel et al. 2020; Voarintsoa et al. 2020) also derived θ values using freshwater aragonitic mollusks (green diamonds, Fig. 8) and synthetic calcite/aragonite (orange crosses, Fig. 8), respectively, using the Pt catalyzed CO_2–O_2 equilibration method. In Figure 8, data from both studies, measured on O_2 derived from CO_2, were converted to the total carbonate using the published a $^{17}O_{CO_2\ (ACID)-carbonate}$ of 1.00535 (Wostbrock et al. 2020a). The $\Delta\Delta'^{17}O_{carb-wt}$ values from both studies are significantly larger and both studies do not report a significant variation with temperature (Fig. 8). Although the reason for the differences between the studies is unknown and warrants further investigation, one possible explanation could be a kinetic fractionation effect during the CO_2–O_2 equilibration method (Fosu et al. 2020; Passey and Levin 2021, this volume) used in both the Bergel et al. (2020)

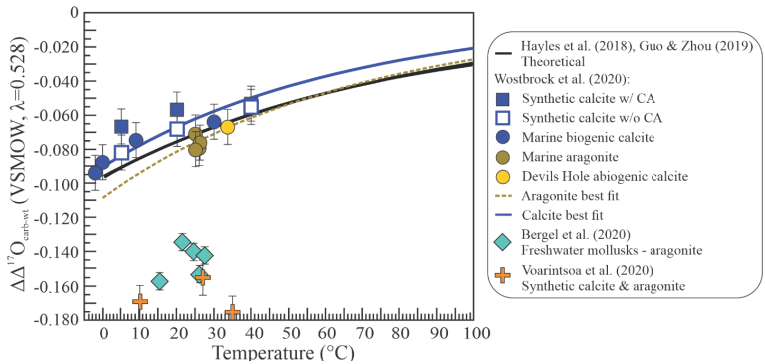

Figure 8. The $\Delta\Delta'^{17}O_{carb-wt}$ as a function of temperature from published studies. Symbols are the average of multiple measurements of a particular sample and error bars are ±1 s.d of average of the reported data in the study. Theoretical $\Delta\Delta'^{17}O_{carb-wt}$–*T* relationship (**thick black line**) from two studies overlap.

and Voarintsoa et al. (2020) studies. Also, the synthesized calcite and calcite/aragonite mixture studies from Wostbrock et al. (2020b) and Voarintsoa et al. (2020), respectively, noted different times before the first crystals appeared during the experiment (3 days vs. 15–30 min (at 35 °C) to 1–2 days (at 10 °C), respectively). The rapid precipitation at 35 °C may have resulted in some kinetic effect where the precipitating carbonate incorporated the oxygen isotope values of the DIC, instead of precipitating in equilibrium with the water. The DIC species were most likely in equilibrium with the water since they waited 24 hours before adding the sodium bicarbonate and calcium chloride solution (Voarintsoa et al. 2020). Nevertheless, this explanation does not explain the differing results between Bergel et al. (2020) which used freshwater aragonitic mollusks and Wostbrock et al. (2020b) who use measured marine calcite shells and aragonite coral, shells, ooids and sediment. Perhaps freshwater aragonitic mollusks tend to form further out of equilibrium with its formation water than marine calcite and aragonite. Again, more research is necessary to better address these differences.

Applications to natural marine samples

Triple oxygen isotope values have also been measured in carbonates found in soil (Passey et al. 2014), tooth enamel and egg shells (Passey et al. 2014), lakes (Passey and Ji 2019) and metamorphic settings (Fosu et al. 2020) and more information can be found in various chapters in this book (e.g., Passey and Levin 2021, this volume). In this chapter, we will focus on calcite and aragonite that formed in a marine setting.

Figure 9 shows the triple oxygen isotope compositions of various marine carbonates from published data (Passey et al. 2014; Fosu et al. 2020; Wostbrock et al. 2020b). Note, Passey et al. (2014) measures the triple oxygen isotope composition of CO_2 evolved from phosphoric acid digestion at 90 °C. Only an $\alpha^{17}O_{CO_2\ (ACID)–carbonate}$ at 25 °C is known (Wostbrock et al. 2020a). Therefore, we use the published $\alpha^{17}O_{CO_2\ (ACID)–carbonate}$ of 1.00535 to correct the CO_2 triple oxygen isotope values to total carbonate, but this correction may not be completely accurate. In this communication we add two additional triple oxygen isotope analyses of Early Triassic ammonites from the Western Interior Seaway of North America (University of New Mexico, Earth and Planetary Sciences collections, donation by Jim Jenks). The Smithian ammonoid (*Anasibirites* sp.) comes from the Crittenden Springs (NE Nevada) locality (Jenks and Brayard 2018). The shell preservation of the ammonoids from this locality is believed to be exceptional, as many specimens have original color patterns preserved. The Spathian ammonoids were collected from the Hot Springs locality from SE Idaho (Guex et al. 2010) and are assigned to the *Columbites* biozone. These ammonoids are commonly found in carbonate concretions. The triple oxygen isotope values of the Smithian ammonite (blue rhombohedron, Fig. 9) are 12.624, 24.227, and –0.094‰ for $\delta^{17}O$, $\delta^{18}O$, and $\Delta'^{17}O$, respectively. The triple oxygen isotope values of the Spathian ammonite (blue pentagon, Fig. 9) are 13.490, 25.867, and –0.084‰ for $\delta^{17}O$, $\delta^{18}O$, and $\Delta'^{17}O$, respectively.

Modern carbonates, six aragonite coral samples (red circle, yellow diamond, and four green squares), four modern brachiopod shells comprised of calcite (green diamonds) and one calcitic oyster (red diamond) are shown in Figure 9. The calcitic oyster appears to be in equilibrium with modern seawater, within reported error, and suggests a formation temperature of ~20 °C, similar to the measured water temperature of 24 °C (Passey et al. 2014). The calcitic brachiopod shells (green diamonds) also plot in equilibrium with the seawater–calcite fractionation curve (Note, these brachiopod samples were among the samples used to derive the fractionation curve in Wostbrock et al. 2020b). Two aragonitic coral samples (red circle and yellow diamond) have triple oxygen isotope values that plot below the calcite–seawater fractionation curve, suggesting a larger aragonite–water fractionation for $\Delta'^{17}O$ than that of calcite–water. This is similar to the conclusions between the $\Delta'^{17}O$ fractionation of calcite–water and aragonite–water presented in Wostbrock et al. (2020b).

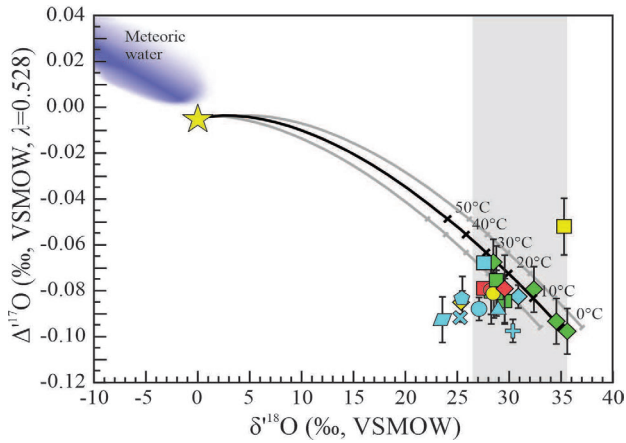

Figure 9. The $\Delta'^{17}O$ values vs. the $\delta'^{18}O$ values of marine carbonates in relation to the equilibrium triple oxygen isotope fractionation curve for calcite (**black curve**) in equilibrium with modern seawater (**yellow star**, $\delta^{18}O = 0$ and $\Delta'^{17}O = -0.005‰$; Luz and Barkan, 2010). Equilibration temperatures are marked along the **black curve**. The seawater curve is bracketed by the modern range (–2 to +2‰) of seawater oxygen isotope compositions for equatorial and mid-latitude oceans (**grey lines**; Schmidt et al. 1999). The range of modern brachiopod $\delta^{18}O$ values (26.5 to 35.5‰) is represented by the **light grey box** (Brand et al. 2019). Data from Wostbrock et al. (2020b) are **green symbols**: modern marine brachiopods (**diamonds**), modern marine aragonite samples (**squares**) and **blue symbols**: Cretaceous belemnite (**diamond**); brachiopods: Mid Ordovician, (X), Silurian (**square**), Mid Devonian (**circle**), Late Pennsylvanian (**triangle**), and Mid Maastrichtian (Late Cretaceous; **cross**); ammonites: Smithian (**rhombohedron**) and Spathian (**pentagon**). Data from Passey et al. (2014) are **red symbols**: Permian brachiopod (**square**), modern estuarine oyster normalized to seawater (**diamond**), modern coral (*Porites porites*, **circle**). Data from Fosu et al. (2020) are **yellow symbols**: modern aragonitic deep sea coral (**diamond**), late Cretaceous chalk comprised of coccoliths (**circle**), modern cold seep high Mg calcite (**square**). An additional cold seep calcite plots off the chart and has a $\Delta'^{17}O$ value of –0.18‰.

Of the fossil carbonate samples shown, only two, a Silurian brachiopod (blue square) and a Cretaceous belemnite from the Peedee formation (PDB, blue diamond), plot close to the seawater fractionation curve (Fig. 9). These samples are consistent with having precipitated in equilibrium with seawater with a $\delta^{18}O$ value of 0 and $\Delta'^{17}O$ value of –0.005‰ (Luz and Barkan 2010). The PDB sample corresponds with a formation temperature of 12 °C while the Silurian brachiopod corresponds to 28 °C. All other samples plot to the left of the seawater–calcite fractionation curve and, therefore, *cannot be in equilibrium with 0‰ seawater*. Assuming that the Phanerozoic seawater value was similar to today (–1 to 0‰), as suggested by the triple oxygen isotope values of the Silurian brachiopod sample and the Cretaceous belemnite, then all of the triple oxygen isotope values of these samples are best explained by diagenesis. Discussion of what these altered samples tell us about the ancient ocean is presented in "*Application to carbonate and silica sediments*".

CONSIDERATIONS NECESSARY TO INTERPRET ANCIENT SEDIMENTS

Traditional oxygen isotope studies have used the oxygen isotope composition of ancient carbonates and silicates to reconstruct the temperature of the seawater over time, as well as other proxies such as phosphates and shales (see Sharp 2017; Bindeman 2021, this volume, for more information on additional proxies). The accuracy of oxygen isotope paleothermometry is critically dependent on the assumed $\delta^{18}O$ value of the ancient ocean. While it is generally agreed upon that the ocean is buffered to its present value by a complex interplay of plate tectonics and erosion (Muehlenbachs and Clayton 1976; Muehlenbachs 1986), the $\delta^{18}O$ value of past seawater is still debated. There is a secular trend seen in the carbonate and silica (chert) record

with decreasing $\delta^{18}O$ values with increasing age (Lowenstam 1961; Degens and Epstein 1962; Keith and Weber 1964; Perry 1967; Knauth and Epstein 1976; Veizer and Hoefs 1976; Knauth and Lowe 1978, 2003; Perry et al. 1978; Popp et al. 1986; Veizer et al. 1986, 1989, 1997, 1999; Lohmann and Walker 1989; Brand 2004; Knauth 2005; Prokoph et al. 2008; Veizer and Prokoph 2015; Ryb and Eiler 2018). See Figure 1 in Zakharov et al. (2021, this volume). For example, the $\delta^{18}O$ value of Archean cherts are generally 15‰ lower than modern (Knauth and Epstein 1976; Knauth and Lowe 1978, 2003; Perry et al. 1978; Winter and Knauth 1992). The explanation for the secular trend falls under three main hypotheses (Degens and Epstein 1962) and a fourth, less talked about hypothesis:

1. **The ocean was warmer in the Archean than it is today** (Knauth and Epstein 1976, 1986; Knauth and Lowe 1978, 2003; Winter and Knauth 1992; Perry and Lefticariu 2007). This hypothesis implies the $\delta^{18}O$ value of seawater remains constant (~0‰) over time and the temperature of Archean seawater was 50–80 °C and cooled over time. Assuming a linear cooling, the warm ocean theory would imply that the Cambrian seawater was about 40–60 °C warmer than modern seawater during the explosion of life, a direct contradiction to reasonable temperature estimates of survivability of most prokaryotes (Brock 1985). Additionally, when applied to the Archean, this hypothesis complicates the faint sun paradox (Sagan and Mullen 1972), although the faint sun paradox itself has been recently called into question (Rosing et al. 2010). Seawater modelling studies based on the oxygen isotope values of altered oceanic crust support this idea that seawater has been buffered to 0‰ for most of Earth′s history (Muehlenbachs and Clayton 1976; Gregory and Taylor 1981; Muehlenbachs 1986; Gregory 1991; Holmden and Muehlenbachs 1993, 1998; Zakharov and Bindeman 2019). Various studies using carbonate clumped isotope (Δ_{47}) values also suggest the ocean was buffered to 0‰, albeit with varying temperature estimates (20–70 °C), since at least the Cambrian (Eiler 2011; Finnegan et al. 2011; Cummins et al. 2014; Ryb and Eiler 2018; Price et al. 2020).

2. **The $\delta^{18}O$ value of seawater was lower in the past** (Perry 1967; Perry and Tan 1972; Veizer and Hoefs 1976; Veizer et al. 1997, 1999; Hren et al. 2009; Veizer and Prokoph 2015). This hypothesis implies the $\delta^{18}O$ value of Archean seawater was as low as −15‰. Models to explain the low $\delta^{18}O$ value of the ancient ocean have been developed by assuming very different ratios of high to low temperature alteration flux rates compared to the modern (Wallmann 2001; Kasting et al. 2006; Jaffrés et al. 2007; Kanzaki 2020). Ocean temperatures would be similar to modern over the geologic rock record. The idea of an ocean with lower $\delta^{18}O$ values than modern seawater is contradicted by oxygen isotope studies of ancient ophiolites, where the oxygen isotope values of the altered rocks is governed by the oxygen isotope value of the hydrothermal water (initially seawater) at an assumed constant temperature over time (Muehlenbachs and Clayton 1976; Gregory and Taylor 1981; Muehlenbachs 1986, 1998; Gregory 1991). Recent seawater oxygen isotope compositional modelling by Sengupta and Pack (2018) suggest that a 100-fold increase of the continental weathering flux rate would be required to lower the ocean to −8‰. The authors could not reconstruct a seawater with the a $\delta^{18}O$ value of −15‰ using any feasible changing scenario of known or estimated flux rates.

3. **Ancient samples have been overprinted by diagenesis** (Gao and Land 1991; Wenzel et al. 2000; Brand 2004; Marin-Carbonne et al. 2012, 2014; Sengupta and Pack 2018; Liljestrand et al. 2020). Diagenetic alteration generally occurs at elevated temperatures and/or in the presence of waters with a lower $\delta^{18}O$ value of seawater (Popp et al. 1986; Lohmann and Walker 1989; Banner and Hanson 1990; Gao and Land 1991; Marshall 1992; Wadleigh and Veizer 1992; Kah 2000; Swart 2015; Ahm et al. 2018). However, there are rare instances where the $\delta^{18}O$ value of the diagenetic fluid may be higher than modern seawater (Grossman et al. 1991), particularly in evaporative basinal porewaters (Swart 2015).

In general, the $\delta^{18}O$ values of older sediments have lower $\delta^{18}O$ values. The argument that diagenesis explains the low $\delta^{18}O$ value of ancient sediments suggests that the diagenesis is a continual process, such that older materials have been more strongly affected than younger ones or that alteration conditions themselves have changed through time.

4. **Hydrothermal systems formed much of the Archean chert record** (De Ronde et al. 1997; Sengupta et al. 2020; Zakharov et al. 2021, this volume). The triple oxygen isotope data are explained by this idea, but some geologic and petrographic evidence does not support high temperature, hydrothermal deposition. For example, some stratigraphic evidence of laterally continuous chert beds and low temperature facies preservation such as rip-up clasts suggest that at least some of the ancient chert was deposited in shallow, near surface settings during the Archean (Knauth 1979; Lowe 1983; Maliva et al. 1989, 2005; Tice et al. 2004; Tice and Lowe 2006; Perry and Lefticariu 2007).

To complicate things further, there are some studies where the $\delta^{18}O$ of seawater is proposed to have been up to 3‰ *higher* in the past (Longinelli et al. 2002, 2003; Johnson and Wing 2020). In summary, the $\delta^{18}O$ value of seawater over the geologic record is still an open question.

Triple oxygen isotope measurements help constrain the fluid in which the silicate or carbonate formed or can help determine if the sample is preserving primary depositional information because samples must fall on a unique curve in $\Delta'^{17}O$–$\delta'^{18}O$ space for a given composition of water (Fig. 2). Departures from this line are explained by changes in the triple oxygen isotope composition of the ocean and/or diagenesis, explained in further detail below. Samples that lie to the left of the seawater equilibrium curve have been altered by a diagenetic fluid of meteoric origin. Samples that lie above the modern seawater equilibration curve have either formed in an ocean with a lower $\delta'^{18}O$–higher $\Delta'^{17}O$ value or, rarely, undergone alteration with a fluid with a higher $\delta^{18}O$ value than seawater. The triple oxygen isotope composition of ancient materials should therefore shed light on which processes might explain their low $\delta^{18}O$ values.

Modelling changing ocean composition in the past

Sengupta and Pack (2018) modeled how the $\Delta'^{17}O$ and $\delta'^{18}O$ values of seawater would change in response to changing rates high- to low-temperature alteration. Similar to Muehlenbachs (1998), they determined that continental weathering and high temperature hydrothermal alteration during seafloor spreading were the two principal fluxes that drive the seawater oxygen isotope change. They obtained a λ value of 0.51 for changing the continental weathering and high temperature seafloor alteration fluxes. Liljestrand et al. (2020) suggested that at least 90% of the total alteration must come from low temperature continental weathering in order to have Archean seawater with a $\delta^{18}O$ value of −15‰. They propose a λ of 0.524 for low temperature seafloor alteration (Liljestrand et al. 2020), slightly higher than the combined high- and low-temperature alteration λ proposed in Sengupta and Pack (2018). Bindeman (2021, this volume) measured the triple oxygen isotope composition of shales and proposes an intermediate λ value of 0.521. For simplicity, we use the λ value of 0.51 in Figure 10 to show how the seawater equilibrium fractionation curve would change over time if low temperature alteration governed Archean seawater oxygen isotope composition. Sediments that formed in equilibrium with a seawater composition plotting on the $\lambda = 0.51$ line would then plot above the modern equilibrium curve (shaded grey region, Fig. 10).

Hypothetical triple oxygen isotope values of samples are shown as circles in Figure 10. The green circle can be interpreted as being in equilibrium with modern seawater. The blue circle could be in equilibrium with seawater with a $\delta'^{18}O$ value of −4‰ and a $\Delta'^{17}O$ value of 0.075‰. The red circle in Figure 5 could only be in equilibrium with the ocean if the $\delta'^{18}O$ value was significantly higher than today as suggested by Johnson and Wing (2020). It is not unreasonable that continental erosion would have been lower in the Archean due to a low abundance of continental crust (Bindeman et al. 2018), in which case the ocean would move

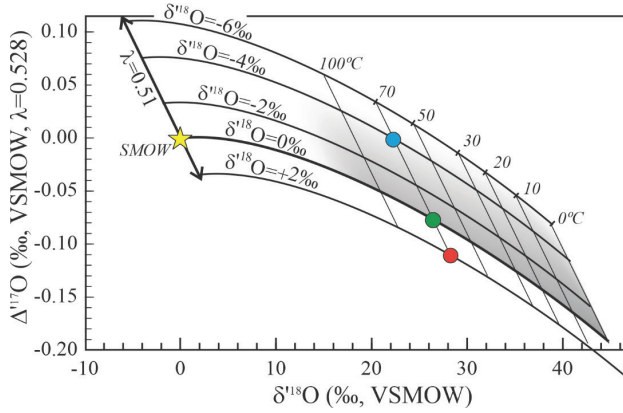

Figure 10. $\Delta'^{17}O$–$\delta'^{18}O$ plot of changing seawater composition. The line labeled $\lambda = 0.51$ is the trajectory of seawater composition for changing high- to low-temperature alteration ratios (Sengupta and Pack 2018). **All circles** represent hypothetical data. The **green circle** is in equilibrium with modern water at 70°C. The **blue circle** is the $\Delta'^{17}O$–$\delta'^{18}O$ value of silica in equilibrium with a modelled lower $\delta'^{18}O_{seawater}$ value of –4‰ at 70 °C. The **red circle** is the $\Delta'^{17}O$–$\delta'^{18}O$ value of silica in equilibrium with a modelled higher $\delta'^{18}O_{seawater}$ value of +2‰ at 70 °C (Johnson and Wing 2020). For similar temperatures of formation, triple oxygen isotope values of silica should have higher $\Delta'^{17}O$ values and lower $\delta^{18}O$ values than modern silica if the $\delta^{18}O$ value of seawater was lower in the past and lower $\Delta'^{17}O$ values and higher $\delta^{18}O$ values than modern silica if the $\delta^{18}O$ value of seawater was higher in the past.

along the $\lambda = 0.51$ line towards higher $\delta^{18}O$ values (Johnson and Wing 2020) and lower $\Delta'^{17}O$ values As discussed below, a shift to higher $\delta^{18}O$ values for the ancient ocean then leads to higher temperature estimates based on the mineral–water fractionations. It is therefore argued that ancient cherts may have formed in high temperature hydrothermal system (De Ronde et al. 1997; Sengupta et al. 2020; Zakharov et al. 2021, this volume). Alternatively, the red circle in Figure 5 may be the result of diagenesis, as explained in the following section.

Modelling triple oxygen isotope trends during diagenesis

Low temperature diagenesis of marine sediments generally drives the $\delta^{18}O$ values lower and $\Delta'^{17}O$ values higher (Sharp et al. 2018). Several variables control the oxygen isotope composition during diagenetic alteration including, temperature, initial rock and fluid oxygen isotope compositions, and the fluid/rock (F/R) ratio. Nevertheless, the $\delta'^{18}O$–$\Delta'^{17}O$ field of most diagenetically altered rock is surprisingly limited (Fig. 11; Sharp et al. 2018).

The effect of alteration can be determined using a simple mass-balance mixing model. A fraction of water is allowed to equilibrate with a rock at a given temperature following Taylor (1978). The bulk composition is given by the equation

$$\delta^x O_{bulk} = X_{water}\,(\delta^x O_{water\ initial}) + (1-X_{water})\,(\delta^x O_{rock\ initial}) \quad (27a)$$

and

$$\delta^x O_{bulk} = X_{water}\,(\delta^x O_{water\ final}) + (1-X_{water})\,(\delta^x O_{rock\ final}) \quad (27b)$$

$\delta^x O$ can be either $\delta^{18}O$ or $\delta^{17}O$. The final $\delta^x O$ value of the rock is determined by the additional equation

$$\alpha^x = \frac{1000 + \delta^x O_{final\,rock}}{1000 + \delta^x O_{final\,water}} \quad (28)$$

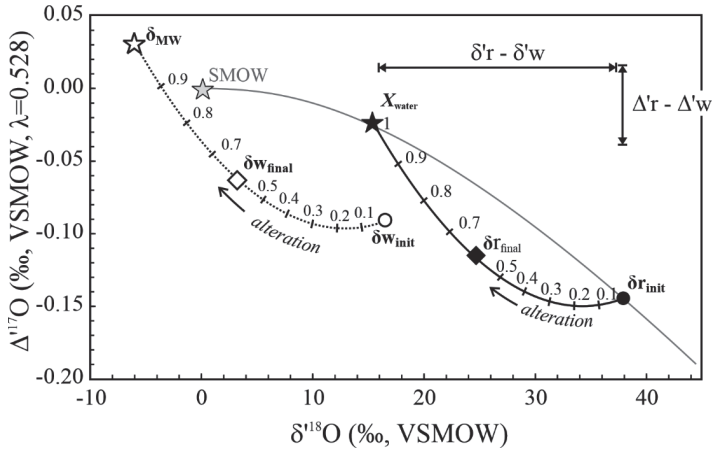

Figure 11. Alteration trajectories in $\Delta'^{17}O$–$\delta'^{18}O$ space. The rock starts at δr_{init} (**black circle**) and moves along the **solid curve** with increasing fluid/rock ratio. The infiltrating fluid has a composition at δ_{MW} (**white star**), equilibrates with rock and has a composition δw_{init} (**white circle**). The re-equilibrated water follows the dotted curved path from δw_{init} towards lower $\delta'^{18}O$ and higher $\Delta'^{17}O$ values as the *F/R* ratio increases. The final rock and water compositions in this example correspond to an X_{water} value of 0.6, resulting in the δw_{final} (**white diamond**) and δr_{final} (**black diamond**) The equilibrium oxygen isotope fractionations at 100 °C are shown by the **doubled arrow lines**.

Combining Equations (27a), (27b), and (28) leads to the relationship between the initial rock and water oxygen isotope compositions, the fluid/rock ratio and the final isotopic composition of the rock:

$$\delta^x O_{\text{rock final}} = \frac{1000X + \alpha\left(X \cdot \delta^x O_{\text{rock initial}} - X \cdot \delta^x O_{\text{water initial}} - \delta^x O_{\text{rock initial}} - 1000X\right)}{\alpha X - \alpha - X} \quad (29)$$

A typical alteration pathway at 100 °C is shown in Figure 11. The fractionation between the water and rock is shown by the arrows δ′r–δ′w and Δ′r–Δ′w. As long as temperature is held constant, these fractionations will not change. The initial rock is silica in equilibrium with seawater water at 20 °C (black circle and δr_{init}). The meteoric water that infiltrates the rock has initial $\delta^{18}O$ and $\Delta'^{17}O$ values of –6 and +0.03‰ (white star and δ_{MW}). The infiltrating meteoric water always has a constant composition (δ_{MW}) and equilibrates with the rock as it enters the system. When the alteration process first begins, an infinitely small amount of water enters the system and equilibrates with the rock. The fraction of oxygen from the water relative to the total water–rock oxygen reservoir is near zero. In the model, this first 'aliquot' of water will equilibrate with the overwhelmingly large oxygen reservoir of rock and have a composition given by δw_{init} (white circle, Fig. 11). This is the oxygen isotope composition of the equilibrated water when the fluid–rock interaction process first begins to take place.

As more fluid enters the system, the F/R ratio increases and the oxygen isotope composition of the fluid and rock track up the solid (rock) and dotted (water) curves. As the F/R ratio approaches an infinite value, the oxygen isotope composition of the fluid is equal to that of infiltrating meteoric water (δ_{MW}). The infiltrating water 'overwhelms' the buffering capacity of the rock. The $\delta'^{18}O$ and $\Delta'^{17}O$ values the rock will be in equilibrium at 100 °C with the δ_{MW} (white star, Fig. 11). The final oxygen isotope composition of the rock at the end of the alteration process is a function of the F/R ratio. In Figure 11, the white and black diamonds illustrate an intermediate condition corresponding to an X_{water} = 0.6 or a fluid–rock ratio of 1.5 (X_{water}/X_{rock} = 0.6/0.4). The variables that control the alteration pathways are the temperature of alteration, the $\delta^{18}O$ and $\Delta'^{17}O$ values of the infiltrating water, and the initial oxygen isotope

composition of the rock (which is a function of its formation temperature). Figure 12 shows various alteration trajectories for different water compositions and temperatures.

In general, we expect to see altered marine rocks lying to the left of the seawater equilibrium curve, shown by the lavender region in Figure 13. This field is generated by considering a wide range of reasonable infiltrating fluid triple oxygen isotope compositions, alteration temperatures, and initial rock triple oxygen isotope (black curves, Fig. 13). For case studies see Herwartz et al. (2015), Zakharov and Bindeman (2019), Chamberlain et al. (2020), and Herwartz (2021, this volume). The alteration field is mostly distinct from the 'changing seawater' field generated by lowering the $\delta^{18}O$ value of ancient seawater by changing high- to low-temperature alteration ratios (shaded grey region, Fig. 13). These two fields—alteration in lavender and

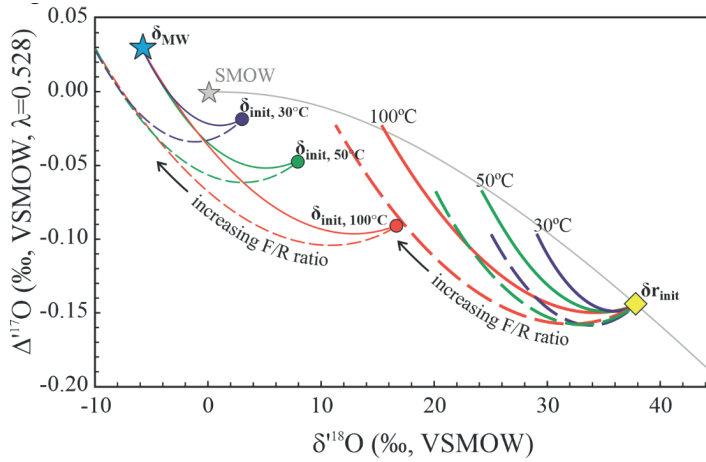

Figure 12. Alteration trajectories for a rock starting with a $\delta'^{18}O$–$\Delta'^{17}O$ of δr_{init}. **Dashed and solid lines** are for interaction with an infiltrating meteoric water (δ_{MW}) with $\delta'^{18}O$ values of −10‰ and −6‰, respectively and $\Delta'^{17}O$ values of 0.03‰. The rock trajectories are **thick curves**, fluids are **thin curves**.

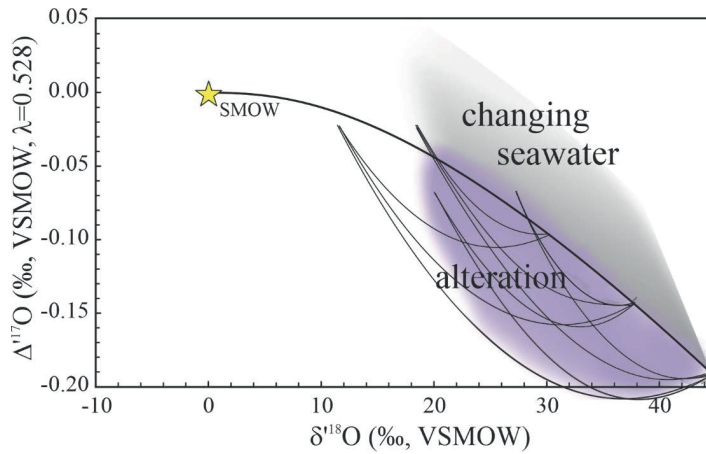

Figure 13. Generalized fields for sedimentary silica. The **lavender field** represents the general region expected for alteration based on numerous trajectories for different water compositions and temperatures (**black curved lines**). The **grey region** is calculated for lower oxygen isotope compositions of seawater predicted if high- to low-temperature alteration ratios changed dramatically in the past.

lowering ocean values in grey—represent the generalized regions where we can expect most sediment phases to plot. Overall, samples that lie below and to the left of the equilibrium line are explained by diagenesis. There are alteration scenarios that would result in a positive shift for both the $\delta^{18}O$ and $\Delta'^{17}O$ values. This may be seen in hot buoyant fluids that infiltrate a cooler overlying sedimentary pile (see final section of this chapter).

Application to carbonate and silica sediments

Phanerozoic calcite. Wostbrock et al. (2020b) reported the triple oxygen isotope values of five ancient brachiopods and one belemnite from the Phanerozoic. Only two samples, a Silurian brachiopod (formation temperature ~28 °C) and a Cretaceous belemnite (formation temperature ~12 °C), have triple oxygen isotope values that can be in equilibrium with seawater similar to a modern ocean oxygen isotope composition (Fig. 9). The remaining brachiopods from that study and the two ammonites presented in this manuscript all have $\delta^{18}O$ and $\Delta'^{17}O$ values that plot to the left of the modern seawater triple oxygen isotope fractionation curve, suggesting alteration by a meteoric water. It is only with the addition of the $\Delta'^{17}O$ value that we are able to conclude that these ancient brachiopods do not preserve triple oxygen isotope compositions and could not have formed in seawater similar to modern oceans (grey box, Fig. 9).

We can use the fluid/rock alteration model to 'see through' the alteration and calculate the original triple oxygen isotope composition of the samples, prior to alteration (Fig. 14). For the Ordovician brachiopod, Wostbrock et al. (2020b) were able to fit the measured triple oxygen isotope data using a meteoric fluid as the alteration fluid with a $\delta^{18}O$ value between −15 and −10‰, a $\Delta'^{17}O$ value of +0.03‰, and an alteration temperature between 35 and 100 °C. Under these conditions, the back-calculated initial $\delta^{18}O$ value of the brachiopod was between 30 and 32.5‰, corresponding to a formation temperature of 10 to 20 °C, assuming the seawater had a similar triple oxygen isotope composition as modern oceans. Using the same fluid–rock mixing model, we calculated the primary composition of the other altered brachiopod and ammonite samples (Fig. 14). All the brachiopod shells formed in water ranging between 10 and 20 °C, similar to the 0–30 °C water temperature range of modern brachiopods (Brand et al. 2019). For the Smithian and Spathian (Early Triassic) ammonites, we find that both ammonites are altered in spite of the high visual preservation quality of the fossil shell. Nevertheless, we can back-calculate formation temperatures of 10 and 20 °C for the Spathian and Smithian age samples, respectively. These agree well with the 10 °C difference suggested using the $\delta^{18}O$ values of conodonts (Sun et al. 2012). Overall, we do not see evidence of lower $\delta^{18}O$ values of the ocean, nor higher temperatures in the Phanerozoic, although the number of samples measured to date is still small.

Ancient silica. Sedimentary bulk silica is found throughout the rock record from 3.5 Ga through to the present day (Knauth 2005). Chert is inherently the product of a diagenetic process where dissolved silica is reprecipitated and evolves from Opal-A to Opal-CT to microcrystalline quartz. Generally, the term "chert" refers to microcrystalline quartz. The amount of time it takes for Opal-A to transform to microcrystalline quartz is still an active area of research (Yanchilina et al. 2020). The ocean has been undersaturated with respect to silica since the appearance of silica-secreting radiolarians and siliceous sponges in the Phanerozoic and later diatoms in the Jurassic. Most Phanerozoic silica deposits originated as biogenic Opal-A, which later transformed to microcrystalline quartz generally in an offshore environment (Maliva et al. 1989; Perry and Lefticariu 2007). Prior to the Phanerozoic, the ocean may have been close to or at silica saturation, and marine silica is thought to have mostly precipitated through abiogenic (or inorganic) processes. Preservation of sedimentary features in Precambrian and earlier outcrops gives credence to the idea that some transformations can occur in the near subsurface not long after deposition (Knauth 1973; Knauth and Lowe 1978; Lowe 1983; Maliva et al. 1989, 2005; Tice et al. 2004; Tice and Lowe 2006; Perry and Lefticariu 2007). The ubiquitous presence of chert throughout geologic time and the assumed lower susceptibility to diagenesis than carbonate has made the oxygen isotope composition of chert an attractive sample to use as a paleo-indicator of ancient seawater.

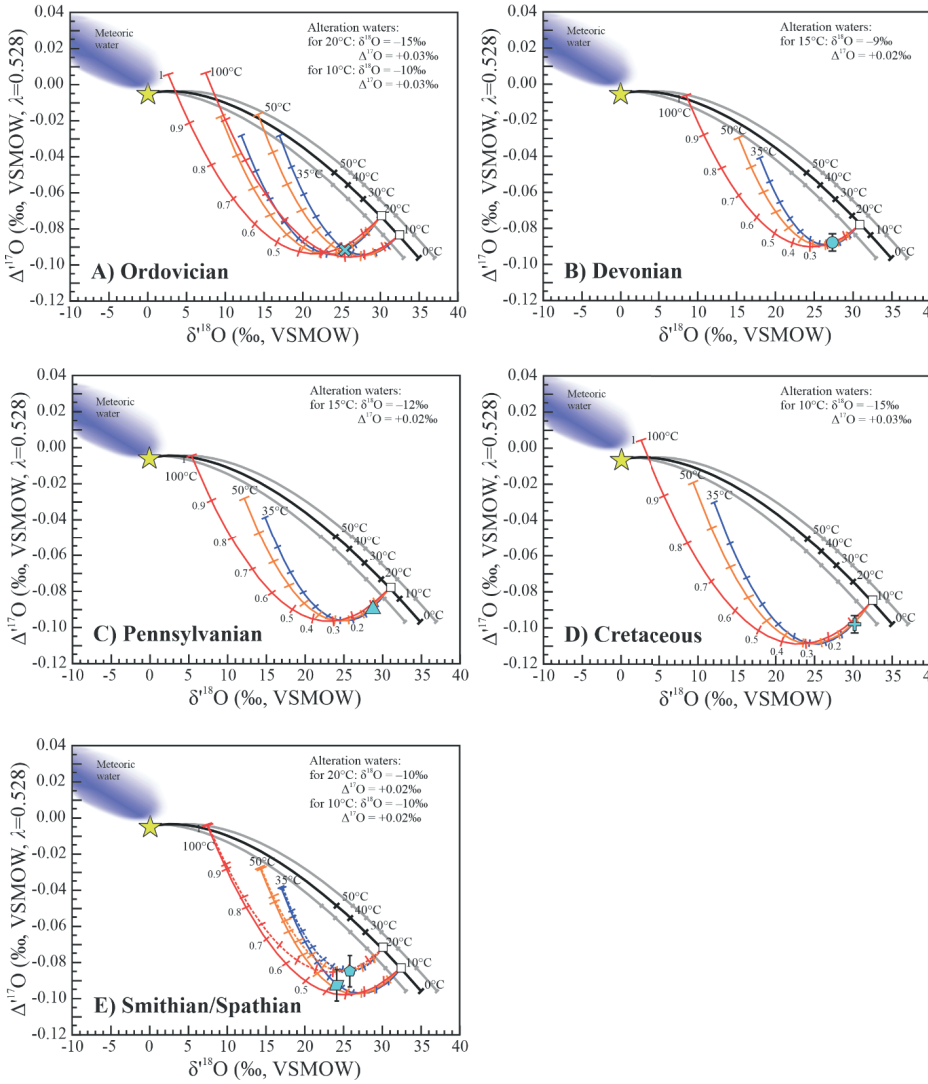

Figure 14. Back-calculated initial triple oxygen isotope compositions of altered brachiopod and ammonite samples. Alteration fluid triple oxygen isotope value are written on each graph and pathways were modelled for alteration temperatures of 35 (**blue lines**), 50 (**orange lines**), and 100 (**red lines**) °C. **A)** The Mid-Ordovician brachiopod formed between 10 and 20 °C. To demonstrate the fact that the fluid–rock interaction model is under constrained, Wostbrock et al. (2020b) used two different alteration fluids to calculate two different potential primary calcite triple oxygen isotope values and show the range of results the model can produce. For **B**–**E**, we only show one potential solution for the fluid–rock mixing model for the sake of simplicity. **B)** The Mid Devonian brachiopod calculated primary calcite triple oxygen isotope composition suggests an initial precipitation temperature of ~18 °C. **C)** The Late Pennsylvanian brachiopod calculated primary calcite triple oxygen isotope composition suggests an initial precipitation temperature of ~15 °C. **D)** The Mid Maastrichtian (Late Cretaceous) brachiopod calculated primary calcite triple oxygen isotope composition suggests an initial precipitation temperature of ~10 °C. **E)** The Smithian ammonite (**rhombohedron**) calculated primary calcite triple oxygen isotope composition suggests an initial precipitation temperature of ~20 °C. The Spathian ammonite (**pentagon**) calculated primary calcite triple oxygen isotope composition suggests an initial precipitation temperature of ~10 °C.

Four studies have published values on the triple oxygen isotope composition of cherts from the Archean through the Phanerozoic (Levin et al. 2014; Liljestrand et al. 2020; Sengupta et al. 2020; Zakharov et al. 2021, this volume) and the results are presented in Figure 15. First, the vast majority of all chert samples that have been measured for triple oxygen isotope analysis plot to the left of the modern silica-seawater equilibrium fractionation line. Perhaps most importantly, all chert samples from the Archean (dark blue icons in Fig. 15) plot at far lower $\delta^{18}O$ values than other samples and to the left of the modern silica–seawater equilibrium fractionation line. The fact that they do not plot above the equilibrium line indicates that their unique $\delta^{18}O$–$\Delta'^{17}O$ values are not due to lower $\delta^{18}O$ seawater compositions related to changing high- to low-temperature alteration ratios (Figs. 12 and 13). Therefore, the secular trend seen in the $\delta^{18}O$ values of chert is not compatible with an Archean seawater $\delta^{18}O$ value of −8 to −15‰ unless the alteration trend of $\lambda = 0.51$ (Sengupta and Pack 2018) is not correct. Other studies suggest higher λ values of 0.521 (Bindeman 2021, this volume) and 0.524 (Liljestrand et al. 2020). Using a λ value of 0.524 and a $\delta^{18}O$ value of −8‰ for the ocean can explain only a few of the Proterozoic chert data (solid red line, Fig. 16) with a formation water temperature of 30 to 40 °C. However, even this high λ value cannot reconcile any Archean chert or the majority of the published chert dataset (Fig. 16).

Almost none of the chert data can be explained by equilibration with a modern seawater oxygen isotope composition. Chert samples from the Phanerozoic presented in Sengupta et al. (2020), represented by the yellow diamonds in Figure 15, are explained by dissolution and equilibrium re-precipitation with a meteoric–marine fluid mixture with a $\delta^{18}O$ value of −3‰ and a $\Delta'^{17}O$ value of +0.010‰ (dashed purple line with purple star, Fig. 15; Sengupta et al. 2020). This implies the samples are preserving a precipitation temperature between 20 and 30 °C, suggesting near-surface dissolution and re-precipitation. Similarly, Zakharov et al. (2021, this volume) suggest the first generation of microcrystalline quartz in a Proterozoic chert sample (light blue crosses in Fig. 14) formed in equilibrium with

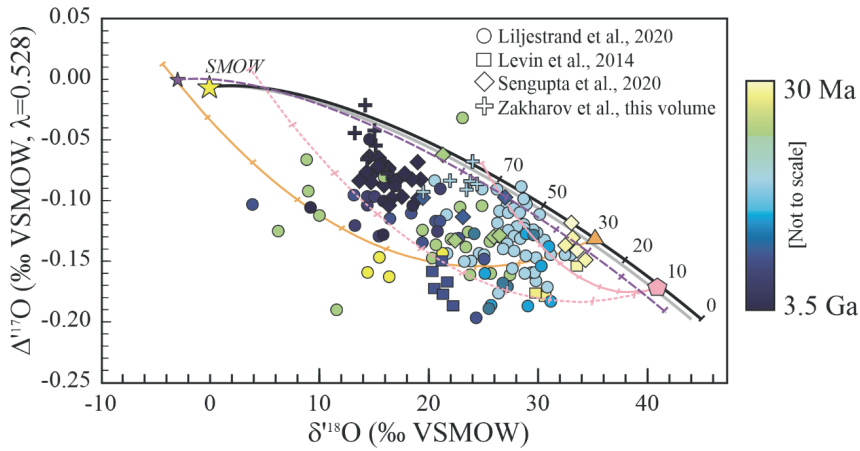

Figure 15. Published $\Delta'^{17}O$ and $\delta'^{18}O$ values of ancient chert from the Archean through Phanerozoic from Levin et al. (2014, **squares**) Liljestrand et al. (2020, **circles**), Sengupta et al. (2020, **diamonds**), Zakharov et al. (2021, this volume, **crosses**). **Yellow colors** are younger cherts while **blue colors** represent older cherts. One interpretation for the chert data suggest alteration by a fluid with a lower triple oxygen isotope value than the modern ocean (SMOW, **yellow star**). Using a fluid–rock mixing model, the precipitation temperature of the primary chert was calculated as 30 °C (Liljestrand et al. 2020; **orange line and triangle**) and 10 °C (Sengupta and Pack 2018; **pink lines and hexagon**). Sengupta et al. (2020) proposed that Phanerozoic chert (**yellow icons**) generally form by dissolution and equilibrium re-precipitation after burial in a meteoric-marine water mixture (**purple star and dashed lines**). The initial formation temperatures are then 30 and 40 °C. Zakharov et al. (2021, this volume) suggests a similar precipitation scenario with pore fluid during the Proterozoic (**light blue icons**) and formation temperatures greater than 60 °C.

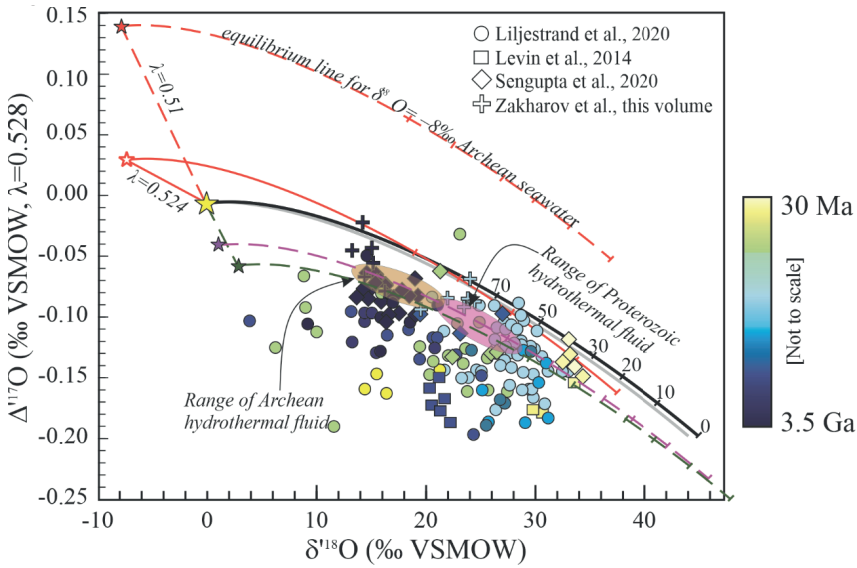

Figure 16. Various seawater triple oxygen isotope compositions can describe published $\Delta'^{17}O$ and $\delta'^{18}O$ values of ancient chert from the Archean through Phanerozoic from Levin et al. (2014, **squares**) Liljestrand et al. (2020, **circles**), Sengupta et al. (2020, **diamonds**), Zakharov et al. (2021, this volume, **crosses**). **Yellow colors** are younger cherts while **blue colors** represent older cherts. The triple oxygen isotope values of chert are not consistent with seawater having had a lower $\delta^{18}O$ value in the past (**red stars**) if corresponding change in $\delta^{18}O$ and $\Delta'^{17}O$ following either the trend with the lowest λ value of 0.51 modelled by Sengupta and Pack (2018; **dashed red line**) or the trend with the highest λ value of 0.524 suggested by Liljestrand et al. (2020; **solid red line**). A possible explanation is that the $\delta^{18}O$ value of seawater was higher in the Archean compared to modern or that Precambrian chert tended to form in a hydrothermal system with a higher $\delta^{18}O$ value than modern seawater. The fluid could have a $\delta^{18}O$ value of +1‰ (**purple star and dashed purple line**) as proposed in Sengupta et al. (2020) and Zakharov et al. (2021, this volume) or have a $\delta^{18}O$ value as high as +3‰ as proposed in Johnson and Wing (2020; **green star and dashed line**). Either seawater $\delta^{18}O$ scenario suggests high formation temperatures between 150 and 300 °C for Archean chert (**orange circle**) and 70 to 150 °C for Proterozoic chert (**purple circle**).

interstitial pore fluid that is similar to slightly lower than the modern seawater oxygen isotope composition at a temperature between 50 and 80 °C, representative of the temperature of early diagenesis. Alteration of Phanerozoic cherts has long been known to commonly occur and are actually probably the norm (Knauth and Epstein 1976). It is not surprising, therefore, to expect alteration by meteoric waters to have occurred in older samples.

All current triple oxygen isotope studies of chert suggest alteration by secondary fluids. Sengupta and Pack (2018) and Liljestrand et al. (2020) suggest the initial precipitation of the silica occurred in seawater with a $\delta^{18}O$ value similar to modern seawater and at temperatures below 30 °C. Both studies used fluid–rock interaction models (Figs. 11 and 12) to calculate primary chert compositions. Liljestrand et al. (2020) constrained the initial silica formation to have occurred at 30 °C, with a subsequent diagenetic alteration at 200 °C with a fluid of −16.5‰. Sengupta and Pack (2018) (using renormalized data from Levin et al. 2014) concluded that alteration by a fluid with a $\delta^{18}O$ value of −6‰ at 50 °C generally explains the Phanerozoic chert data. In contrast, an alteration fluid of 10‰ at 180 °C explains the Archean cherts and a chert precipitation temperature of −10 °C.

Sengupta et al. (2020) used a Bayesian model to calculate two different alteration scenarios for their Archean and Proterozoic chert data. For the Archean samples they separated samples

into two groups, one with $\delta^{18}O$ values between 13 and 16‰ and one group with $\delta^{18}O$ values between 18.7 and 19.3‰. For the first Archean group, they concluded that the silica precipitated in seawater with an oxygen isotope composition similar to modern seawater, and was subsequently altered by a fluid with a $\delta^{18}O$ value of −16.5‰ at an alteration temperature of 50 °C and W/R ratio of 1. Their Bayesian model was inconclusive on initial silica precipitation temperature. For the second group of Archean chert, the Bayesian model again predicted initial precipitation in seawater with an oxygen isotope composition similar to modern at 80 °C and was subsequently altered with a fluid with a $\delta^{18}O$ value of –14‰ at either 50 or 150 °C. The Bayesian model was ambiguous as to the W/R ratio. Proterozoic cherts fit within both Archean diagenetic models. Sensitivity in the Bayesian model allows for the initial silica from either the Archean or Proterozoic samples to have formed in temperatures as low as 10 °C (Sengupta et al. 2020).

Although diagenesis can explain the above data, Sengupta et al. (2020) also consider the hypothesis that the Archean and Proterozoic samples are retaining primary oxygen isotope values in which the chert equilibrated with a fluid that had a higher $\delta^{18}O$ value than modern seawater (Fig. 16). This idea is also favored by Zakharov et al. (2021, this volume). Sengupta et al. (2020) acknowledge that they cannot distinguish between whether the samples formed in seawater with higher $\delta^{18}O$ and lower $\Delta'^{17}O$ values than modern seawater (Johnson and Wing 2020) due to higher hydrothermal water flux in the Archean (Isley 1995; Lowell and Keller 2003) or whether the samples formed in high temperature hydrothermal vent fluids with ambient seawater similar to modern (Bindeman et al. 2018; Zakharov and Bindeman 2019; Peters et al. 2020).

Zakharov et al. (2021, this volume) use a modern hydrothermal vent in Iceland as an analog to an Archean vent-like setting with fluids having a $\delta^{18}O$ value of 0.9 to 1.6‰ (De Ronde et al. 1997; Farber et al. 2015) and temperatures between 150 and 300 °C. Sengupta et al. (2020) suggest a similar fluid (either vent or ambient seawater) oxygen isotope composition with a $\delta^{18}O$ value of +1‰ and $\Delta'^{17}O$ value of −0.040‰, corresponding to a temperature of formation for the Archean cherts of 150 to 220 °C and 75–150 °C for Proterozoic cherts (purple star and dashed line, Fig. 16). They explain the lower Proterozoic fluid temperatures result from a lowering of the geothermal gradient. Johnson and Wing (2020) argue that, due to the absence of continents, the Archean ocean could have a $\delta^{18}O$ value as high as +3‰ (green star and dashed line, Fig. 16). Following a $\lambda \approx 0.51$ for the changing seawater trend presented in Sengupta and Pack (2018), an Archean seawater with a $\delta^{18}O$ value of +3‰ would then have a $\Delta'^{17}O$ value of about −0.05‰. Seawater with a $\delta^{18}O$ value of +3‰ also fits the Archean and Proterozoic chert samples (blue symbols in Fig. 16) at similar temperatures proposed by Sengupta et al. (2020) and Zakharov et al. (2021, this volume). Interestingly, seawater with a $\delta^{18}O$ value of +3‰ does not fit the majority of the Phanerozoic chert samples. If the hypothesis that most Precambrian chert formed in seawater with a higher $\delta^{18}O$ value than modern, perhaps chert formation processes in the Phanerozoic were different, due to the presence of marine silica-secreting organisms (Maliva et al. 1989, 2005; Perry and Lefticariu 2007).

Overall, most Archean and Proterozoic chert that has currently been measured for triple oxygen isotope values could have formed or been altered by high-temperature vent fluids with $\delta^{18}O$ values higher than modern seawater. Alternatively, the data can be explained by having initial silica precipitation at less than 30 °C in marine water with a modern oxygen isotope composition, and subsequent diagenetic alteration by meteoric waters (Sengupta and Pack 2018; Liljestrand et al. 2020). This latter interpretation agrees with the classic $\delta^{18}O$–δD study of Knauth and Epstein (1976) where altered samples have a $\delta D/\delta^{18}O$ slope similar to the meteoric water line. Examining Archean and Proterozoic chert that preserve sedimentary facies, such as draping and rip up clasts, indicating formation in a near-shore marine setting at or near the seafloor would provide additional information. Based on the data published thus far, however, we conclude that the data do not suggest Archean or Proterozoic seawater with a lower $\delta^{18}O$ value than modern.

TRIPLE OXYGEN ISOTOPES OF COEXISTING QUARTZ AND CALCITE

We can combine the $\Delta\Delta'^{17}O$ fractionation equations (Eqns. 24 and 26) for quartz–water and calcite–water to derive the equilibrium oxygen isotope fractionation between quartz and calcite (Fig. 17). The θ_{qz-cc} values are less than those of quartz–water or calcite–water. At 0°C, our calculated θ_{qz-cc} of 0.518 compares well with the theoretical estimate of 0.520 (Hayles et al. 2018).

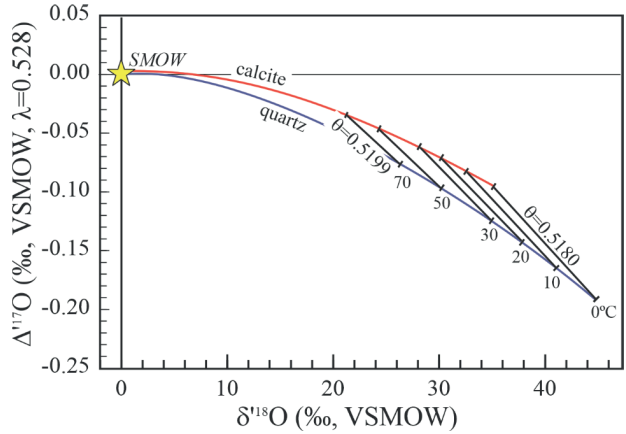

Figure 17. $\Delta'^{17}O$–$\delta'^{18}O$ plot for quartz and calcite and the equilibrium θ_{qz-cc} values from 0 to 70 °C.

We consider three carbonate lithologies that contain authigenic quartz: the well-known Herkimer Diamond quartz crystals hosted in carbonate (New York, USA), doubly terminated quartz crystals in early–middle transition Triassic marine pelagic limestone (North Dobrogea, Romania), and chert nodules from a Cretaceous limestone (Étretat, France). The Herkimer Diamond and marine pelagic limestone from North Dobrogea, Romania both contain glassy, optically clear quartz crystals. The Romanian samples do not contain sponge spicules, although they are found elsewhere in the section, suggesting that the quartz crystals are the product of dissolution and reprecipitation of the sponge spicules. The Étretat, France sample is not glassy quartz, but rather fine-grained chert (data from Pack and Herwartz 2014). The other two samples are data from Sharp et al. (2016) and all data are normalized to the same San Carlos olivine scale (see Sharp and Wostbrock 2021, this volume).

The two authigenic quartz samples can be explained by dissolution of amorphous silica and recrystallization as quartz during a period of meteoric water infiltration (Fig. 18). If a small amount of meteoric water entered the system, it could dissolve the reactive, metastable amorphous silica and cause it to reprecipitate without appreciably interacting with the host calcite. Using a simple mass balance model following Equation (29), we can calculate the initial $\Delta'^{17}O$ and $\delta'^{18}O$ values of the amorphous silica for both the Romanian and New York samples with differing F/R ratios and reaction temperatures. For the Romanian samples, the $\delta^{18}O$ value of the calcite is ~33.3‰ (not shown in Fig. 18), corresponding to a formation temperature of ~10 °C. Two reactions paths are illustrated at diagenesis temperatures of 45 and 70 °C using a starting quartz value in equilibrium with seawater at 10 °C. For the Herkimer samples, alteration temperatures approaching 100 °C are expected (not shown in Fig. 18). Calculated F/R ratios for both samples are high, but it is important to recognize that this is the *effective* F/R ratio. If the calcite had only minimal interaction with the infiltrating fluid, then the ratio of oxygen in the fluid to quartz could be high even if there was only a small amount of fluid.

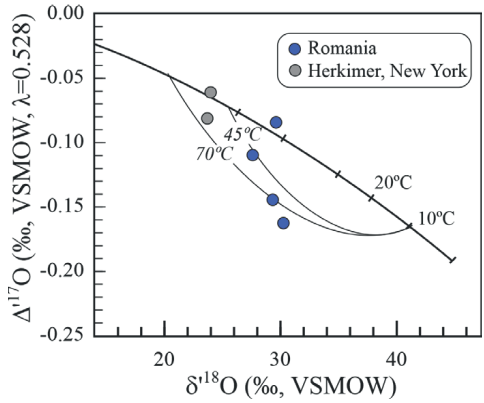

Figure 18. Isotopic compositions of authigenic euhedral quartz crystals hosted in carbonates. The isotope data suggest some degree of alteration by meteoric fluids. Pathways for interaction between a sample formed at ~10 °C (as evidenced by carbonate $\delta^{18}O$ values and a meteoric fluid ($\delta^{18}O = -6‰$, $\Delta'^{17}O = 0.03‰$. Alteration paths shown for temperatures of 45 °C and 70 °C.

The French chert samples plot above the equilibrium curve for quartz and seawater (Fig. 19). It is not possible to explain this sample in terms of equilibrium with ocean water or diagenesis with meteoric water. Instead, we suggest a scenario of fluids migrating from deeper hotter sections into overlying sediments. The overall process shown in Figure 19 is the following: First, a carbonate is precipitated at 35 °C in equilibrium with seawater at composition ① illustrated by the red diamond. The sample is buried and heated to 100 °C. Interstitial fluid in equilibrium with the heated carbonate re-equilibrates to an oxygen isotope composition at ② (red pentagon). The curve between ① and ② is the oxygen isotope equilibrium curve for carbonates with the origin at the carbonate value (position ①; blue solid line). This fluid then buoyantly infiltrates the overlying sediment at a lower temperature and precipitates quartz at ③ (red hexagon). The black curve between ② and ③ is the oxygen isotope equilibrium curve for quartz with a fluid at ②. The geological scenario is reasonable and provides an explanation for how samples can plot above the mineral–seawater equilibrium curve.

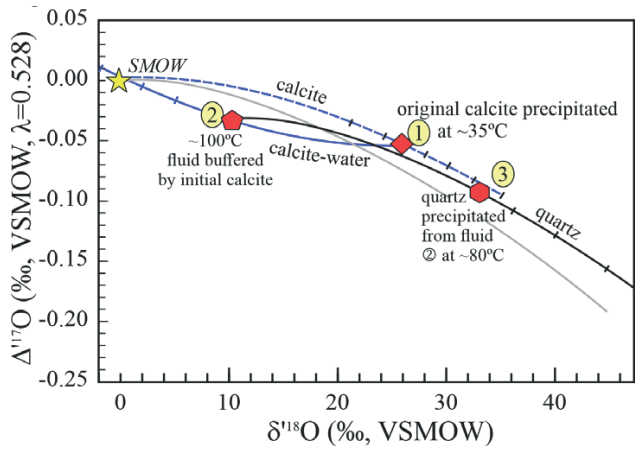

Figure 19. Possible reaction sequence to explain the high $\Delta'^{17}O$ value (**red circle**) of carbonate-hosted chert from Étretat, France (data from Pack and Herwartz 2014). 1) Carbonates form with an isotopic composition at ①. 2) The sample is heated and the pore fluid buffered by the carbonate is shown at ②. 3) The fluid infiltrates the cooler overlying sediment and precipitates quartz at ③. The **grey curve** shows the equilibrium quartz–water fractionation with seawater.

CONCLUSION

Recent studies have clearly demonstrated the usefulness in making triple oxygen isotope measurements compared to measuring the $\delta^{18}O$ value alone. Triple oxygen isotope measurements serve as a unique tool that can determine equilibrium vs. non-equilibrium vs. alteration processes. Triple oxygen isotope compositions allow for a definitive test for diagenesis. If a sample does not lie on the equilibrium curve, it is not in equilibrium with modern seawater.

The silica–water triple oxygen isotope fractionation system appears to be well constrained. Inconsistencies remain in published carbonate–water triple oxygen isotope fractionation values, probably due to the different methods used to obtain the triple oxygen isotope values. Nevertheless, application of the calcite–water or quartz–water triple oxygen isotope fractionation curves to samples where the formation water is no longer present allows us to constrain the temperatures of formation and conditions of diagenesis. A fluid–rock mixing model can be used to 'see through' alteration and calculate the primary oxygen isotope compositions of silicate and carbonate rocks. Applying this model to silicates and carbonates from the geologic record shows that the low $\delta^{18}O$ values of the ancient samples do not appear to be related to changing ocean temperatures and/or ocean isotope values. Instead, Phanerozoic carbonate and chert samples are better explained by diagenesis and Proterozoic and older chert can be explained by either diagenesis or precipitation in hydrothermal fluid.

ACKNOWLEDGEMENTS

J.A.G.W and Z.S acknowledges support from NSF GRFP grant DGE-1418062, NSF EAR 1551226, and NSF EAR 1747703. We thank Jim Jenks, Viorel Atudorei, and UNM EPS collections for the Smithian and Spathian ammonite samples. The authors also thank constructive reviews by Weifu Guo and Page Chamberlain and the patience of editors Ilya Bindeman and Andreas Pack.

REFERENCES

Adkins JF, Boyle EA, Curry WB, Lutringer A (2003) Stable isotopes in deep-sea corals and a new mechanism for "vital effects". Geochim Cosmochim Acta 67:1129–1143

Adnew GA, Hofmann ME, Paul D, Laskar A, Surma J, Albrecht N, Pack A, Schwieters J, Koren G, Peters W, Röckmann T (2019) Determination of the triple oxygen and carbon isotopic composition of CO_2 from atomic ion fragments formed in the ion source of the 253 Ultra high-resolution isotope ratio mass spectrometer. Rapid Commun Mass Spectrom 33:1363–1380

Ahm A-SC, Bjerrum CJ, Blättler CL, Swart PK, Higgins JA (2018) Quantifying early marine diagenesis in shallow-water carbonate sediments. Geochim Cosmochim Acta 236:140–159

Bajnai D, Fiebig J, Tomašových A, Milner Garcia S, Rollion-Bard C, Raddatz J, Löffler N, Primo-Ramos C, Brand U (2018) Assessing kinetic fractionation in brachiopod calcite using clumped isotopes. Sci Rep 8:533

Banner JL, Hanson GN (1990) Calculation of simultaneous isotopic and trace element variations during water–rock interaction with applications to carbonate diagenesis. Geochim Cosmochim Acta 54:3123–3137

Barkan E, Musan I, Luz B (2015) High-precision measurements of $\delta^{17}O$ and $^{17}O_{excess}$ of NBS19 and NBS18. Rapid Commun Mass Spectrom 29:2219–2224

Beck WC, Grossman EL, Morse JW (2005) Experimental studies of oxygen isotope fractionation in the carbonic acid system at 15°, 25°, and 40°C. Geochim Cosmochim Acta 69:3493–3503

Bergel SJ, Barkan E, Stein M, Affek HP (2020) Carbonate $^{17}O_{excess}$ as a paleo-hydrology proxy: Triple oxygen isotope fractionation between H_2O and biogenic aragonite, derived from freshwater mollusks. Geochim Cosmochim Acta 275:36–47

Bigeleisen J, Goeppert Mayer M (1947) Calculation of equilibrium constants for isotopic exchange reactions. J Chem Phys 15:261–267

Bijma J, Spero HJ, Lea DW (1999) Reassessing foraminiferal stable isotope geochemistry: impact of the oceanic carbonate system (experimental results). *In*: Use of Proxies in Paleoceanography: Examples from the South Atlantic. Fischer G, Wefer G, (eds). Springer Berlin Heidelberg, p 489–512

Bindeman IN (2021) Triple oxygen isotopes in evolving continental crust, granites, and clastic sediments. Rev Mineral Geochem 86:241–290

Bindeman IN, Zakharov DO, Palandri J, Greber ND, Dauphas N, Retallack GJ, Hofmann A, Lackey JS, Bekker A (2018) Rapid emergence of subaerial landmasses and onset of a modern hydrologic cycle 2.5 billion years ago. Nature 557:545–548

Bottinga Y, Javoy M (1973) Comments on oxygen isotope geothermometry. Earth Planet Sci Lett 20:250–265

Brand U (2004) Carbon, oxygen and strontium isotopes in Paleozoic carbonate components: an evaluation of original seawater-chemistry proxies. Chem Geol 204:23–44

Brand U, Bitner MA, Logan A, Azmy K, Crippa G, Angiolini L, Colin P, Griesshaber E, Harper EM, Ruggiero ET, Häussermann V (2019) Brachiopod-based oxygen-isotope thermometer: Update and review. Rivista Italiana di Paleontologia e Stratigrafia 125:775–787

Brandriss ME, O′Neil JR, Edlund MB, Stoermer EF (1998) Oxygen isotope fractionation between diatomaceous silica and water. Geochim Cosmochim Acta 62:1119–1125

Brock TD (1985) Life at high temperatures. Science 230:132–138

Cao X, Liu Y (2011) Equilibrium mass-dependent fractionation relationships for triple oxygen isotopes. Geochim Cosmochim Acta 75:7435–7445

Carlson PE, Noronha AL, Banner JL, Jenson JW, Moore MW, Partin JW, Deininger M, Breecker DO, Bautista KK (2020) Constraining speleothem oxygen isotope disequilibrium driven by rapid CO_2 degassing and calcite precipitation: Insights from monitoring and modeling. Geochim Cosmochim Acta 284:222–238

Chamberlain CP, Ibarra DE, Lloyd MK, Kukla T, Sjostrom D, Gao Y, Sharp ZD (2020) Triple oxygen isotope systematics of meteoric hydrothermal systems and implications for paleoaltimetry. Geochem Perspect Lett in press

Clayton RN, Kieffer SW (1991) Oxygen isotopic thermometer calibrations. *In*: Stable Isotope Geochemistry: A Tribute to Samuel Epstein. Vol 3. Taylor HPJ, O′Neil JR, Kaplan IR, (eds). Lancaster Press, Inc., San Antonio, p 3–10

Coplen TB (2007) Calibration of the calcite–water oxygen-isotope geothermometer at Devils Hole, Nevada, a natural laboratory. Geochim Cosmochim Acta 71:3948–3957

Criss RE (1991) Temperature dependence of isotopic fractionation factors. *In*: Stable Isotope Geochemistry: A Tribute to Samuel Epstein. Vol 3. Taylor HPJ, O′Neil JR, Kaplan IR, (eds). The Geochemical Society, San Antonio, p 11–16

Crundwell FK (2017) On the mechanism of the dissolution of quartz and silica in aqueous solutions. ACS Omega 2:1116–1127

Cummins RC, Finnegan S, Fike DA, Eiler JM, Fischer WW (2014) Carbonate clumped isotope constraints on Silurian ocean temperature and seawater $\delta^{18}O$. Geochim Cosmochim Acta 140:241–258

Daëron M, Drysdale RN, Peral M, Huyghe D, Blamart D, Coplen TB, Lartaud F, Zanchetta G (2019) Most Earth-surface calcites precipitate out of isotopic equilibrium. Nat Commun 10:429

De Ronde CEJ, Channer DMd, Faure K, Bray CJ, Spooner ETC (1997) Fluid chemistry of Archean seafloor hydrothermal vents: Implications for the composition of circa 3.2 Ga seawater. Geochim Cosmochim Acta 61:4025–4042

Degens ET, Epstein S (1962) Relationship between O^{18}/O^{16} ratios in coexisting carbonates, cherts, and diatomites 1: Geological Notes. AAPG Bull 46:534–542

Devriendt LS, Watkins JM, McGregor HV (2017) Oxygen isotope fractionation in the $CaCO_3$–DIC–H_2O system. Geochim Cosmochim Acta 214:115–142

Dietzel M, Tang J, Leis A, Köhler SJ (2009) Oxygen isotopic fractionation during inorganic calcite precipitation—Effects of temperature, precipitation rate and pH. Chem Geol 268:107–115

Dodd JP, Sharp ZD (2010) A laser fluorination method for oxygen isotope analysis of biogenic silica and a new oxygen isotope calibration of modern diatoms in freshwater environments. Geochim Cosmochim Acta 74:1381–1390

Dodd JP, Sharp ZD, Fawcett PJ, Brearley AJ, McCubbin FM (2012) Rapid post-mortem maturation of diatom silica oxygen isotope values. Geochem Geophys Geosyst 13:Q09014

Eiler JM (2011) Paleoclimate reconstruction using carbonate clumped isotope thermometry. Quat Sci Rev 30:3575–3588

Epstein S, Buchsbaum R, Lowenstam HA, Urey HC (1951) Carbonate–water isotopic temperature scale. Geol Soc Am Bull 62:417–426

Epstein S, Buchsbaum R, Lowenstam HA, Urey HC (1953) Revised carbonate–water isotopic temperature scale. Geol Soc Am Bull 64:1315–1326

Farber K, Dziggel A, Meyer FM, Prochaska W, Hofmann A, Harris C (2015) Fluid inclusion analysis of silicified Palaeoarchaean oceanic crust—A record of Archaean seawater? Precambrian Res 266:150–164

Finnegan S, Bergmann K, Eiler JM, Jones DS, Fike DA, Eisenman I, Hughes NC, Tripati AK, Fischer WW (2011) The magnitude and duration of late Ordovician–early Silurian glaciation. Science 331:903

Fosu BR, Subba R, Peethambaran R, Bhattacharya SK, Ghosh P (2020) Technical note: Developments and applications in triple oxygen isotope analysis of carbonates. ACS Earth Space Chem 4:702–710

Gao G, Land LS (1991) Geochemistry of Cambro–Ordovician Arbuckle limestone, Oklahoma: Implications for diagenetic $\delta^{18}O$ alteration and secular $\delta^{13}C$ and $^{87}Sr/^{86}Sr$ variation. Geochim Cosmochim Acta 55:2911–2920

Garrels RM, Christ CL (1965) Solutions, Minerals, and Equilibria. Freeman, Cooper and Co, San Francisco, CA

Gonfiantini R, Panichi C, Tongiorgi E (1968) Isotopic disequilibrium in travertine deposition. Earth Planet Sci Lett 5:55–58

Gregory RT (1991) Oxygen isotope history of seawater revisited: Timescales for boundary event changes in the oxygen isotope compostion of seawater. *In*: Stable Isotope Geochemistry: A Tribute to Samuel Epstein. H.P Taylor J, O′Neil JR, Kaplan IR, (eds). The Geochemical Society, San Antonio, p 65–76

Gregory RT, Taylor HP (1981) An oxygen isotope profile in a section of Cretaceous oceanic crust, Samail Ophiolite, Oman: Evidence for $\delta^{18}O$ buffering of the oceans by deep (>5 km) seawater-hydrothermal circulation at mid-ocean ridges. J Geophys Res 86:2737–2755

Grossman El, Zhang C, Yancey TE (1991) Stable-isotope stratigraphy of brachiopods from Pennsylvanian shales in Texas. GSA Bulletin 103:953–965

Guex J, Hungerbuhler A, Jenks J, O'Dogherty L, Atudorei V, Taylor D, Bucher H, Bartoloni A (2010) Spathian (Lower Triassic) ammonoids from western USA (Idaho, California, Utah and Nevada). Memoires de Geologie (Lausanne) 49:82

Guo W, Zhou C (2019) Triple oxygen isotope fractionation in the DIC–H_2O–CO_2 system: A numerical framework and its implications. Geochim Cosmochim Acta 246:541–564

Hayles JA, Gao C, Cao X, Liu Y, Bao H (2018) Theoretical calibration of the triple oxygen isotope thermometer. Geochim Cosmochim Acta 235:237–245

Herwartz D (2021) Triple oxygen isotope variations in Earth's crust. Rev Mineral Geochem 86:291–322

Herwartz D, Pack A, Krylov D, Xiao YL, Muehlenbachs K, Sengupta S, Di Rocco T (2015) Revealing the climate of snowball Earth from $\Delta^{17}O$ systematics of hydrothermal rocks. PNAS 112:5337–5341

Hill PS, Tripati AK, Schauble EA (2014) Theoretical constraints on the effects of pH, salinity, and temperature on clumped isotope signatures of dissolved inorganic carbon species and precipitating carbonate minerals. Geochim Cosmochim Acta 125:610–652

Holmden C, Muehlenbachs K (1993) The $^{18}O/^{16}O$ ratio of 2-billion-year-old seawater inferred from ancient oceanic crust. Science 259:1733–1736

Hren MT, Tice MM, Chamberlain CP (2009) Oxygen and hydrogen isotope evidence for a temperate climate 3.42 billion years ago. Nature 462:205–208

Hulston JR, Thode HG (1965) Variations in the S^{33}, S^{34}, and S^{36} contents of meteorites and their relation to chemical and nuclear effects. J Geophys Res 70:3475–3484

Isley AE (1995) Hydrothermal plumes and the delivery of iron to Banded Iron Formation. J Geol 103:169–185

Jaffrés JBD, Shields GA, Wallmann K (2007) The oxygen isotope evolution of seawater: A critical review of a long-standing controversy and an improved geological water cycle model for the past 3.4 billion years. Earth Sci Rev 83:83–122

Jenks J, Brayard A (2018) Smithian (Early Triassic ammonoids from Crittenden Springs, Elko County, Nevada: Taphonomy, Biostratigraphy and Biogeography. New Mexico Museum of Natural Sciences Bulletin 78:175 pp.

Johnson BW, Wing BA (2020) Limited Archaean continental emergence reflected in an early Archaean ^{18}O-enriched ocean. Nat Geosci 13:243–248

Kah L (2000) Depositional $\delta^{18}O$ signatures in Proterozoic dolostones: constraints on seawater chemistry and early diagenesis. *In*: Carbonate Sedimentation and Diagenesis in the Evolving Precambrian World. Vol 67. Grotzinger JP, James NP, (eds). SEPM Special Publication, Tulsa, OK, USA, p 345–360

Kanzaki Y (2020) Interpretation of oxygen isotopes in Phanerozoic ophiolites and sedimentary rocks. Geochemistry, Geophysics, Geosystems 21:e2020GC009000

Karhu J, Epstein S (1986) The implication of the oxygen isotope records in coexisting cherts and phosphates. Geochim Cosmochim Acta 50:1745–1756

Kasting JF, Tazewell Howard M, Wallmann K, Veizer J, Shields G, Jaffrés J (2006) Paleoclimates, ocean depth, and the oxygen isotopic composition of seawater. Earth Planet Sci Lett 252:82–93

Keith ML, Weber JN (1964) Carbon and oxygen isotopic composition of selected limestones and fossils. Geochim Cosmochim Acta 28:1787–1816

Kim ST, O'Neil JR (1997) Equilibrium and nonequilibrium oxygen isotope effects in synthetic carbonates. Geochim Cosmochim Acta 61:3461–3475

Kim S-T, Mucci A, Taylor BE (2007) Phosphoric acid fractionation factors for calcite and aragonite between 25 and 75 °C: Revisited. Chem Geol 246:135–146

Kita I, Taguchi S, Matsubaya O (1985) Oxygen isotope fractionation between amorphous silica and water at 34–93 °C. Nature 314:83–84

Knauth LP (1973) Oxygen and hydrogen isotope ratios in cherts and related rocks. PhD California Institute of Technology

Knauth LP (1979) A model for the origin of chert in limestone. Geology 7:274–277

Knauth LP (2005) Temperature and salinity history of the Precambrian ocean: Implications for the course of microbial evolution. Palaeogeogr Palaeoclimatol Palaeoecol 219:53–69

Knauth LP, Epstein S (1976) Hydrogen and oxygen isotope ratios in nodular and bedded cherts. Geochim Cosmochim Acta 40:1095–1108

Knauth LP, Lowe DR (1978) Oxygen isotope geochemistry of cherts from the Onverwacht Group (3.4 Ga), Transvaal, South Africa, with implication for secular variations in the isotopic composition of cherts. Earth Planet Sci Lett 41:209–222

Knauth LP, Lowe DR (2003) High Archean climatic temperature inferred from oxygen isotope geochemistry of cherts in the 3.5 Ga Swaziland Supergroup, South Africa. GSA Bull 115:566–580

Krauskopf KB (1956) Dissolution and precipitation of silica at low temperatures. Geochim Cosmochim Acta 10:1–26

Leclerc AJ, Labeyrie L (1987) Temperature dependence of the oxygen isotopic fractionation between diatom silica and water. Earth Planet Sci Lett 84:69–74

Levin NE, Raub TD, Dauphas N, Eiler JM (2014) Triple oxygen isotope variations in sedimentary rocks. Geochim Cosmochim Acta 139:173–189

Liljestrand FL, Knoll AH, Tosca NJ, Cohen PA, Macdonald FA, Peng Y, Johnston DT (2020) The triple oxygen isotope composition of Precambrian chert. Earth Planet Sci Lett 537:116167

Lohmann KC, Walker JCG (1989) The $\delta^{18}O$ record of Phanerozoic abiotic marine calcite cements. Geophys Res Lett 16:319–322

Longinelli A, Iacumin P, Ramigni M (2002) $\delta^{18}O$ of carbonate, quartz and phosphate from belemnite guards: implications for the isotopic record of old fossils and the isotopic composition of ancient seawater. Earth Planet Sci Lett 203:445–459

Longinelli A, Wierzbowski H, Di Matteo A (2003) $\delta^{18}O_{(PO43-)}$ and $\delta^{18}O_{(CO32-)}$ from belemnite guards from Eastern Europe: implications for palaeoceanographic reconstructions and for the preservation of pristine isotopic values. Earth Planet Sci Lett 209:337–350

Lowe DR (1983) Restricted shallow-water sedimentation of Early Archean stromatolitic and evaporitic strata of the Strelley Pool Chert, Pilbara Block, Western Australia. Precambrian Res 19:239–283

Lowell RP, Keller SM (2003) High-temperature seafloor hydrothermal circulation over geologic time and archean banded iron formations. Geophys Res Lett 30:1391

Lowenstam HA (1961) Mineralogy, O^{18}/O^{16} ratios, and strontium and magnesium contents of recent and fossil brachiopods and their bearing on the history of the oceans. J Geol 69:241–260

Loyd SJ, Sample J, Tripati RE, Defliese WF, Brooks K, Hovland M, Torres M, Marlow J, Hancock LG, Martin R, Lyons T (2016) Methane seep carbonates yield clumped isotope signatures out of equilibrium with formation temperatures. Nat Commun 7:12274

Luz B, Barkan E (2010) Variations of $^{17}O/^{16}O$ and $^{18}O/^{16}O$ in meteoric waters. Geochim Cosmochim Acta 74:6276–6286

Mahata S, Bhattacharya SK, Wang C-H, Liang M-C (2013) Oxygen isotope exchange between O_2 and CO_2 over hot platinum: An innovative technique for measuring $\delta^{17}O$ in CO_2. Anal Chem 85:6894–6901

Maliva RG, Knoll AH, Siever R (1989) Secular change in chert distribution; a reflection of evolving biological participation in the silica cycle. PALAIOS 4:519–532

Maliva RG, Knoll AH, Simonson BM (2005) Secular change in the Precambrian silica cycle: Insights from chert petrology. GSA Bull 117:835–845

Marin-Carbonne J, Chaussidon M, Robert F (2012) Micrometer-scale chemical and isotopic criteria (O and Si) on the origin and history of Precambrian cherts: Implications for paleo-temperature reconstructions. Geochim Cosmochim Acta 92:129–147

Marin-Carbonne J, Robert F, Chaussidon M (2014) The silicon and oxygen isotope compositions of Precambrian cherts: A record of oceanic paleo-temperatures? Precambrian Res 247:223–234

Marshall JD (1992) Climatic and oceanographic isotopic signals from the carbonate rock record and their preservation. Geol Mag 129:143–160

McConnaughey T (1989) ^{13}C and ^{18}O isotopic disequilibrium in biological carbonates: II. *In vitro* simulation of kinetic isotope effects. Geochim Cosmochim Acta 53:163–171

McCrea JM (1950) On the isotopic chemistry of carbonates and a paleotemperature scale. J Chem Phys 18:849–857

Mickler PJ, Banner JL, Stern L, Asmerom Y, Edwards RL, Ito E (2004) Stable isotope variations in modern tropical speleothems: Evaluating equilibrium vs. kinetic isotope effects Geochim Cosmochim Acta 68:4381–4393

Mickler PJ, Stern LA, Banner JL (2006) Large kinetic isotope effects in modern speleothems. GSA Bull 118:65–81

Miller MF (2002) Isotopic fractionation and the quantification of ^{17}O anomalies in the oxygen three-isotope system: an appraisal and geochemical significance. Geochim Cosmochim Acta 66:1881–1889

Mills GA, Urey HC (1940) The kinetics of isotopic exchange between carbon dioxide, bicarbonate ion, carbonate ion and water 1. J Am Chem Soc 62:1019–1026

Muehlenbachs K (1986) Alteration of the oceanic crust and the ^{18}O history of seawater. Rev Mineral Geochem 16:425–444

Muehlenbachs K (1998) The oxygen isotopic composition of the oceans, sediments and the seafloor. Chem Geol 145:263–273

Muehlenbachs K, Clayton RN (1976) Oxygen isotope composition of the oceanic crust and its bearing on seawater. J Geophys Res 81:4365–4369

O'Neil JR, Clayton RN, Mayeda TK (1969) Oxygen isotope fractionation in divalent metal carbonates. J Chem Phys 51:5547–5558

Pack A, Herwartz D (2014) The triple oxygen isotope composition of the Earth mantle and understanding $\Delta^{17}O$ variations in terrestrial rocks and minerals. Earth Planet Sci Lett 390:138–145

Passey BH, Ji H (2019) Triple oxygen isotope signatures of evaporation in lake waters and carbonates: A case study from the western United States. Earth Planet Sci Lett 518:1–12

Passey BH, Levin NE (2021) Triple oxygen isotopes in meteoric waters, carbonates, and biological apatites: implications for continental paleoclimate reconstruction. Rev Mineral Geochem 86:429–462

Passey BH, Hu H, Ji H, Montanari S, Li S, Henkes GA, Levin NE (2014) Triple oxygen isotopes in biogenic and sedimentary carbonates. Geochim Cosmochim Acta 141:1–25

Perry EC (1967) The oxygen isotope chemistry of ancient cherts. Earth Planet Sci Lett 3:62–66

Perry EC, Lefticariu L (2007) 7.05—Formation and geochemistry of precambrian cherts. *In*: Treatise on Geochemistry. Holland HD, Turekian KK, (eds). Pergamon, Oxford, p 1–21

Perry EC, Jr., Tan FC (1972) Significance of oxygen and carbon isotope variations in early Precambrian cherts and carbonate rocks of southern Africa. GSA Bull 83:647–664
Perry EC, Ahmad SN, Swulius TM (1978) The Oxygen Isotope Composition of 3,800 M.Y. Old Metamorphosed Chert and Iron Formation from Isukasia, West Greenland. J Geol 86:223–239
Peters STM, Szilas K, Sengupta S, Kirkland CL, Garbe-Schönberg D, Pack A (2020) >2.7 Ga metamorphic peridotites from southeast Greenland record the oxygen isotope composition of Archean seawater. Earth Planet Sci Lett 544:116331
Popp BN, Anderson TF, Sandberg PA (1986) Brachiopods as indicators of original isotopic compositions in some Paleozoic limestones. Geol Soc Am Bull 97:1262–1269
Price GD, Bajnai D, Fiebig J (2020) Carbonate clumped isotope evidence for latitudinal seawater temperature gradients and the oxygen isotope composition of Early Cretaceous seas. Palaeogeogr Palaeoclimatol Palaeoecol 109777
Prokoph A, Shields GA, Veizer J (2008) Compilation and time-series analysis of a marine carbonate $\delta^{18}O$, $\delta^{13}C$, $^{87}Sr/^{86}Sr$ and $\delta^{34}S$ database through Earth history. Earth Sci Rev 87:113–133
Rosing MT, Bird DK, Sleep NH, Bjerrum CJ (2010) No climate paradox under the faint early Sun. Nature 464:744–747
Ryb U, Eiler JM (2018) Oxygen isotope composition of the Phanerozoic ocean and a possible solution to the dolomite problem. PNAS 115:6602–6607
Sagan C, Mullen G (1972) Earth and Mars: Evolution of atmospheres and surface temperatures. Science 177:52–56
Sakai S, Matsuda S, Hikida T, Shimono A, McManus JB, Zahniser M, Nelson D, Dettman DL, Yang D, Ohkouchi N (2017) High-precision simultaneous $^{18}O/^{16}O$, $^{13}C/^{12}C$, and $^{17}O/^{16}O$ analyses for microgram quantities of $CaCO_3$ by tunable infrared laser absorption spectroscopy. Anal Chem 89:11846–11852
Schauble EA, Young ED (2020) Mass dependence of equilibrium oxygen isotope fractionation in carbonate, nitrate, oxide, perchlorate, phosphate, silicate, and sulfate minerals. Rev Mineral Geochem 86
Schmidt M, Botz R, Stoffers P, Anders T, Bohrmann G (1997) Oxygen isotopes in marine diatoms: A comparative study of analytical techniques and new results on the isotope composition of recent marine diatoms. Geochim Cosmochim Acta 61:2275–2280
Schmidt G, Bigg G, Rohling E (1999) Global seawater oxygen-18 database. http://datagissnasagov/o18data
Schmidt M, Botz R, Rickert D, Bohrmann G, Hall SR, Mann S (2001) Oxygen isotopes of marine diatoms and relations to opal-A maturation. Geochim Cosmochim Acta 65:201–211
Sengupta S, Pack A (2018) Triple oxygen isotope mass balance for the Earth′s oceans with application to Archean cherts. Chem Geol 495:18–26
Sengupta S, Peters STM, Reitner J, Duda J-P, Pack A (2020) Triple oxygen isotopes of cherts through time. Chem Geol 554:119789
Shackleton NJ, Wiseman JDH, Buckley HA (1973) Non-equilibrium isotopic fractionation between seawater and planktonic foraminiferal tests. Nature 242:177–179
Sharma T, Clayton RN (1965) Measurement of O^{18}/O^{16} ratios of total oxygen of carbonates. Geochim Cosmochim Acta 29:1347–1353
Sharp ZD (2017) Principles of Stable Isotope Geochemistry, 2nd Edition. Open Educational Resources, Albuquerque, NM
Sharp ZD, Wostbrock JAG (2021) Standardization for the triple oxygen isotope system: waters, silicates, carbonates, air, and sulfates. Rev Mineral Geochem 86:179–196
Sharp ZD, Gibbons JA, Maltsev O, Atudorei V, Pack A, Sengupta S, Shock EL, Knauth LP (2016) A calibration of the triple oxygen isotope fractionation in the SiO_2–H_2O system and applications to natural samples. Geochim Cosmochim Acta 186:105–119
Sharp ZD, Wostbrock JAG, Pack A (2018) Mass-dependent triple oxygen isotope variations in terrestrial materials. Geochem Perspect Lett 7:27–31
Shemesh A, Charles CD, Fairbanks RG (1992) Oxygen isotopes in biogenic silica: global changes in ocean temperature and isotopic composition. Science 256:1434–1436
Shemesh A, Burckle LH, Hays JD (1995) Late Pleistocene oxygen isotope records of biogenic silica from the Atlantic sector of the Southern Ocean. Paleoceanography 10:179–196
Silverman DN (1973) Carbonic anhydrase catalyzed oxygen-18 exchange between bicarbonate and water. Arch Biochem Biophys 155:452–457
Spero HJ, Bijma J, Lea DW, Bemis BE (1997) Effect of seawater carbonate concentration on foraminiferal carbon and oxygen isotopes. Nature 390:497–500
Sun Y, Joachimski MM, Wignall PB, Yan C, Chen Y, Jiang H, Wang L, Lai X (2012) Lethally hot temperatures during the early Triassic greenhouse. Science 338:366–370
Swart PK (2015) The geochemistry of carbonate diagenesis: The past, present and future. Sedimentology 62:1233–1304
Taylor HP (1978) Oxygen and hydrogen isotope studies of plutonic granitic rocks. Earth Planet Sci Lett 38:177–210
Thiemens MH (2006) History and applications of mass-independent isotope effects. Ann Rev Earth Planet Sci 34:217–262
Tice MM, Lowe DR (2006) The origin of carbonaceous matter in pre-3.0 Ga greenstone terrains: A review and new evidence from the 3.42 Ga Buck Reef Chert. Earth Sci Rev 76:259–300
Tice M, Bostick B, Lowe D (2004) Thermal history of the 3.5–3.2 Ga Onverwacht and Fig Tree Groups, Barberton greenstone belt, South Africa, inferred by Raman microspectroscopy of carbonaceous material. Geology 32:37–40
Tremaine DM, Froelich PN, Wang Y (2011) Speleothem calcite farmed *in situ*: Modern calibration of $\delta^{18}O$ and $\delta^{13}C$ paleoclimate proxies in a continuously-monitored natural cave system. Geochim Cosmochim Acta 75:4929–4950

Tyler JJ, Sloane HJ, Rickaby REM, Cox EJ, Leng MJ (2017) Post-mortem oxygen isotope exchange within cultured diatom silica. Rapid Commun Mass Spectrom 31:1749–1760

Uchikawa J, Zeebe RE (2012) The effect of carbonic anhydrase on the kinetics and equilibrium of the oxygen isotope exchange in the CO_2–H_2O system: Implications for $\delta^{18}O$ vital effects in biogenic carbonates. Geochim Cosmochim Acta 95:15–34

Urey HC (1947) The thermodynamic properties of isotopic substances. J Chem Soc:562–581

Urey HC, Epstein S, McKinney CR (1951) Measurement of paleotemperatures and temperatures of the Upper Cretaceous of England, Denmark, and the southeastern United States. Geol Soc Am Bull 62:399–416

Veizer J, Hoefs J (1976) The nature of O^{18}/O^{16} and C^{13}/C^{12} secular trends in sedimentary carbonate rocks. Geochim Cosmochim Acta 40:1387–1395

Veizer J, Prokoph A (2015) Temperatures and oxygen isotopic composition of Phanerozoic oceans. Earth Sci Rev 146:92–104

Veizer J, Fritz P, Jones B (1986) Geochemistry of brachiopods: Oxygen and carbon isotopic records of Paleozoic oceans. Geochim Cosmochim Acta 50:1679–1696

Veizer J, Hoefs J, Lowe DR, Thurston PC (1989) Geochemistry of Precambrian carbonates: II. Archean greenstone belts and Archean sea water. Geochim Cosmochim Acta 53:859–871

Veizer J, Bruckschen P, Pawellek F, Diener A, Podlaha OG, Carden GA, Jasper T, Korte C, Strauss H, Azmy K, Ala D (1997) Oxygen isotope evolution of Phanerozoic seawater. Palaeogeogr Palaeoclimatol Palaeoecol 132:159–172

Veizer J, Ala D, Azmy K, Bruckschen P, Buhl D, Bruhn F, Carden GA, Diener A, Ebneth S, Godderis Y, Jasper T (1999) $^{87}Sr/^{86}Sr$, $\delta^{13}C$ and $\delta^{18}O$ evolution of Phanerozoic seawater. Chem Geol 161:59–88

Voarintsoa NRG, Barkan E, Bergel S, Vieten R, Affek HP (2020) Triple oxygen isotope fractionation between $CaCO_3$ and H_2O in inorganically precipitated calcite and aragonite. Chem Geol 539:119500

Wadleigh MA, Veizer J (1992) $^{18}O^{16}O$ and $^{13}C^{12}C$ in lower Paleozoic articulate brachiopods: Implications for the isotopic composition of seawater. Geochim Cosmochim Acta 56:431–443

Wallmann K (2001) The geological water cycle and the evolution of marine $\delta^{18}O$ values. Geochim Cosmochim Acta 65:2469–2485

Watkins JM, Nielsen LC, Ryerson FJ, DePaolo DJ (2013) The influence of kinetics on the oxygen isotope composition of calcium carbonate. Earth Planet Sci Lett 375:349–360

Wenzel B, Lécuyer C, Joachimski MM (2000) Comparing oxygen isotope records of silurian calcite and phosphate—$\delta^{18}O$ compositions of brachiopods and conodonts. Geochim Cosmochim Acta 64:1859–1872

Winter BL, Knauth LP (1992) Stable isotope geochemistry of cherts and carbonates from the 2.0 Ga gunflint iron formation: implications for the depositional setting, and the effects of diagenesis and metamorphism. Precambrian Res 59:283–313

Wostbrock JAG, Sharp ZD, Sanchez-Yanez C, Reich M, van den Heuvel DB, Benning LG (2018) Calibration and application of silica–water triple oxygen isotope thermometry to geothermal systems in Iceland and Chile. Geochim Cosmochim Acta 234:84–97

Wostbrock JAG, Cano EJ, Sharp ZD (2020a) An internally consistent triple oxygen isotope calibration of standards for silicates, carbonates and air relative to VSMOW2 and SLAP2. Chem Geol 533:119432

Wostbrock JAG, Brand U, Coplen TB, Swart PK, Carlson SJ, Sharp ZD (2020b) Calibration of carbonate–water triple oxygen isotope fractionation: seeing through diagenesis in ancient carbonates. Geochim Cosmochim Acta 288:369–388

Yanchilina AG, Yam R, Kolodny Y, Shemesh A (2020) From diatom opal-A $\delta^{18}O$ to chert $\delta^{18}O$ in deep sea sediments. Geochim Cosmochim Acta 268:368–382

Zakharov DO, Bindeman IN (2019) Triple oxygen and hydrogen isotopic study of hydrothermally altered rocks from the 2.43–2.41 Ga Vetreny belt, Russia: An insight into the early Paleoproterozoic seawater. Geochim Cosmochim Acta 248:185–209

Zakharov DO, Marin-Carbonne J, Alleon J, Bindeman IN (2021)Triple oxygen isotope trend recorded by Precambrian cherts: a perspective from combined bulk and in situ secondary ion probe measurements. Rev Mineral Geochem 86:323–365

Zeebe RE (1999) An explanation of the effect of seawater carbonate concentration on foraminiferal oxygen isotopes. Geochim Cosmochim Acta 63:2001–2007

Zeebe RE (2014) Kinetic fractionation of carbon and oxygen isotopes during hydration of carbon dioxide. Geochim Cosmochim Acta 139:540–552

Zheng Y-F (1991) Calculation of oxygen isotope fractionation in metal oxides. Geochim Cosmochim Acta 55:2299–2307